Unique signatures of the Rashba effect in magnetooptical properties of 2D semiconductors

Peter C. Sercel[1,*] and Alexander L. Efros[2,†]

[1] *Center for Hybrid Organic Inorganic Semiconductors for Energy, Golden, Colorado 80401, United States*

[2] *Center for Computational Materials Science, U.S. Naval Research Laboratory, Washington D.C. 20375, United States*

We have shown theoretically that giant magnetic circular dichroism (MCD) should be observed at the absorption band edge of two-dimensional (2D) semiconductors exhibiting Rashba splitting in the presence of a magnetic field perpendicular to the 2D layers. This feature has been found in calculated interband σ^+ and σ^- light absorption coefficients for transitions between the Landau levels (LLs) of the conduction and valence bands. The giant MCD signal is shown to be connected with an unusual magnetic field dependence of the lowest LL in the presence of the Rashba term. A second unique signature of Rashba splitting is a reduction of the exciton diamagnetic shift created by the Rashba terms. We show that these terms lead to the characteristic Rashba exciton dispersion with minima at non-zero momentum. The analysis of the exciton dispersion at non-zero momentum conducted by Gor'kov and Dzaloshinskii shows that variable separation leads to mixed magneto-impulse terms. These terms lead to a *negative* diamagnetic shift which should be observed in the exciton photoluminescence which occurs from the dispersion minimum.

* pcsercel@gmail.com

† sasha.efros@nrl.navy.mil

I. INTRODUCTION

Interband magnetooptical measurements are a commonly accepted way to measure energy band parameters of bulk semiconductors[1] and two - dimensional semiconductor layers [2, 3]. In the case that the exciton binding energy, E_b is rather small $\sim 5-10\,\mathrm{meV}$ it is easy to reach a magnetic field, B for which the electron cyclotron energy, $\hbar\omega_e \gg E_b$, where $\omega_e = eB/m_e c$ with e the electron charge, m_e the effective mass of the electron, c the speed of light, and $\hbar$ the reduced Plank constant. In this limit, the absorption spectrum created by interband optical transitions between Landau levels of the conduction and valence bands consists of multiple allowed transitions whose energy increases with magnetic field. Theoretical analysis of these interband spectra, whose transitions have the form of a fan spreading out with increasing magnetic field, allows the extraction of the energy band parameters, such as effective masses and g factors of electrons and holes and their anisotropy, as well as the non-parabolicity of the electron and hole spectra, which is commonly characterized by the Kane energy parameter.[4] This analysis, however, requires well -resolved interband optical transitions which can be realized only when $\hbar\omega_e > \Gamma$, where Γ is the spectral line width. If the spectra are not resolved, experimentalists use various differential techniques, such as magnetic circular dichroism (MCD), which measure the collective difference between the absorption coefficients for σ^+ and σ^- polarized light.[5]

In the opposite case when $\hbar\omega_e < E_b$, which is common in structures with large exciton binding energy, the interband magnetooptical measurements allow determination of the Zeeman splitting and diamagnetic shifts of the exciton lines.[1–3] The analysis of the experimental data involves extraction of the electron and hole g factors from the Zeeman splitting, and exciton parameters such as the exciton radius, the reduced exciton mass $\mu = (1/m_e + 1/m_h)^{-1}$, where m_h is the hole effective mass, *etc.*, from the exciton spectra and diamagnetic shifts.

Breaking the inversion symmetry of 2D layers by external or intrinsic electric field, semiconductor crystal structure or by asymmetry of the 2D layer surfaces could generate Rashba-Bychkov terms acting on the carriers in the conduction, $\hat{H}_R^e$, and valence, $\hat{H}_R^h$, bands: [6, 7]

$$\hat{H}_R^{e,h} = \frac{\alpha_{e,h}}{\hbar}[\hat{\boldsymbol{\sigma}}^{e,h} \times \hat{\boldsymbol{p}}^{e,h}] \cdot \hat{\boldsymbol{z}} \; = \alpha_{e,h}\left(\hat{k}_y^{e,h}\hat{\sigma}_x^{e,h} - \hat{k}_x^{e,h}\hat{\sigma}_y^{e,h}\right) \; , \tag{1}$$

where $\hat{\boldsymbol{p}}^{e,h}$ and $\hat{\boldsymbol{k}}^{e,h}$ are the momentum operators and wave vectors, $\hat{\boldsymbol{\sigma}}^{e,h}$ are Pauli matrices for the conduction electrons (e) and valence band holes (h) respectively, and $\hat{\boldsymbol{z}}$ is the unit

vector normal to the surface of the 2D layer. In the expressions above, the Rashba coefficients for the electron and hole, $\alpha_{e,h}$, are related to the respective Rashba energies, $E_R^{e,(h)}$, by,

$$E_R^{e,(h)} = \alpha_{e(h)}^2 m_{e(h)}/(2\hbar^2) \tag{2}$$

The magnitude and sign of the Rashba coefficients play an important role in several physical phenomena, for example in potential creation of the ground bright exciton state [8] or providing the efficient electric dipole spin resonance.[9] Could this information be extracted from interband magneto-optical measurements?

This obviously can be done in the strong magnetic field limit for which $\hbar\omega_{e,h} \gg E_b$ and multiple inter-band optical transitions are well resolved ($\hbar\omega_{e,h} \gg \Gamma$). Due to Rashba terms, the magnetic field behavior of the Landau levels are strongly modified from the standard parabolic case, for which the Landau level energies increase linearly with increasing magnetic field and are equidistant from each other.[6] The magnetic field dependence of these levels, together with detailed analysis of the inter-band optical transitions, will be provided later in the paper.

In the weak magnetic field limit, $\hbar\omega_{e,h} < E_b$, and in the absence of Rashba splitting, the effect of the magnetic field on excitons is described by the Zeeman interaction and the diamagnetic shift. Note the exciton levels are split by the electron - hole exchange interaction; the level order for the 1S exciton at $B = 0$ is shown in Fig.1 panel **a**, which shows the exciton center-of-mass dispersion in this case, assuming approximate tetragonal symmetry. While all of the fine structure levels experience a diamagnetic shift, linear-in-magnetic field Zeeman splitting occurs only between the degenerate fine structure levels with angular momentum projection ± 1, which have transition dipoles in the X, Y plane (with corresponding labels in Fig.1). The other levels, Z, whose transition dipole is oriented perpendicular to the layer plane, and D, which is the dark singlet exciton, experience a quadratic Zeeman shift with magnetic field owing to the zero-field fine structure splitting.[10–12]. These behaviors can be observed in absorption or reflection.

However, the standard analysis of the magneto-optical spectra just outlined does not provide a full description of the Rashba exciton, which is created in structures with large Rashba terms in the conduction or valence bands. In this situation, the analysis of the

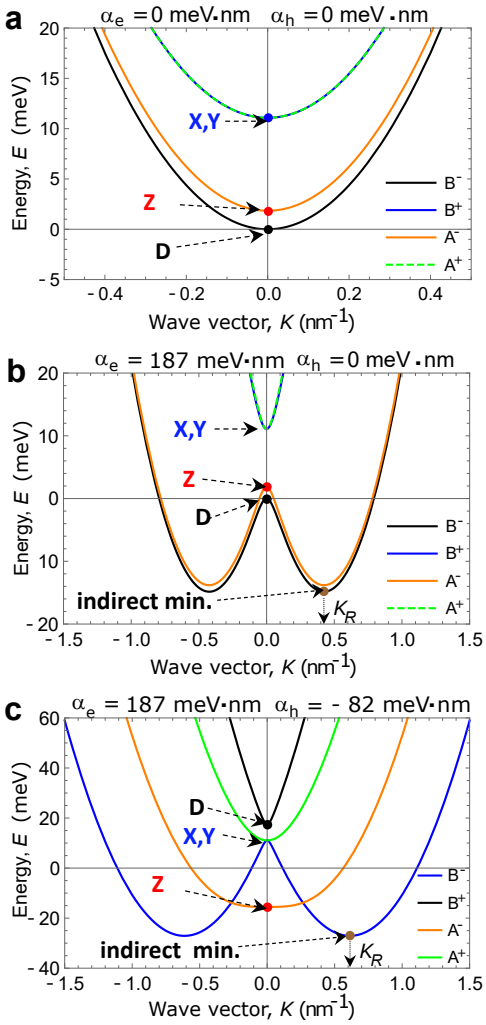

FIG. 1. Dispersion of the 1S Rashba exciton state in a single-layer 2D hybrid organic- inorganic perovskite (HOIP) having approximate tetragonal symmetry, in the absence of a magnetic field. In panel **a** there is no Rashba effect in either the conduction or valence bands; while panel **b** shows the exciton dispersion with non-zero Rashba coefficient α_e only in the conduction band. In panel **c** the Rashba coefficient for the hole is also non-zero; α_e, α_h have opposite signs resulting in a level order inversion between the Z and D exciton. See Appendix B and Eqs. (B7)-(B8) for details of the calculation. The dark exciton (D) dispersion (B^- panels **a** and **b**; B^+ in panel **c**) is plotted with black lines, while the dispersion of the two bright X and Y excitons (A^+/ B^+ in panels **a,b**; A^+/ B^- in panel **c**) are shown in green and blue. Finally, the dispersion of the Z exciton (A^-) is shown with orange lines. In panels **b** and **c**) the Rashba coefficients are not zero. As a result, the exciton dispersion has an "indirect" minimum at $K = K_R \neq 0$, marked in each panel. The exciton dispersion at $K = 0$ is split by the electron-hole exchange interaction. Parameters used in these calculations are listed in Table I and Table A1.

exciton at momentum equal to zero (wave vector $K = 0$ in Fig. 1) proceeds as described above, although if Rashba terms are present in both the conduction and valence bands, the zero field splitting and level order can be affected as shown in Refs. [13, 14] and summarized in Appendix B. This situation is shown in Fig. 1 panel **c** where the electron and hole Rashba coefficients α_e, α_h are both non-zero and have opposite signs, corresponding to co-helical spin textures [15] in the conduction and value bands, as expected from DFT calculations [16], resulting in a level order inversion between the Z and D exciton. Away from $K = 0$, the dispersion of the Rashba excitons is strongly affected by the Rashba terms and is much more complex than in inversion-symmetric semiconductors. This is shown in Fig.1 panel **b**, which depicts the dispersion for the case with non-zero Rashba coefficient α_e only in the conduction band, and in panel **c**, where the Rashba coefficient for the hole is also non-zero. At $K \neq 0$ the dispersion of the excitons is shown by the curves labelled $A^{\pm}$ and $B^{\pm}$ in Fig. 1 whose energies, $E_A^{\pm}(K)$ and $E_B^{\pm}(K)$, respectively, are calculated in Appendix B in Eqs. (B7)-(B8). These equations give the exciton dispersion both with, and without, Rashba splitting. Most importantly for our discussion is that the exciton dispersion in the presence of Rashba splitting has minima at the center-of-mass momentum $K_R \neq 0$[13, 14] as shown in Fig. 1 panels **b** and **c**. In this case, the exciton photoluminescence can occur from the exciton dispersion minima via phonon assisted recombination. Due to the high density of exciton states near the dispersion minima[14] the phonon-assisted excitation of these states may be also be observable in absorption. As we will show below, the diamagnetic shift of the exciton at the dispersion minima is different from that connected with the direct exciton at $K = 0$. The difference in the diamagnetic shifts for the phonon -assisted transition and phononless lines has been observed already experimentally.[17]

In this paper we show theoretically that a MCD signal could be used for measurement of the Rashba terms in the case that interband optical transitions between Landau levels are not resolved. We show that Rashba terms lead to a giant MCD signal near the band edge. For weak magnetic fields, we calculate the diamagnetic shift of the Rashba exciton connected with its indirect dispersion minimum and show that this can be significantly smaller than the diamagnetic shift of the exciton at $K = 0$. For all of the model calculations shown in this study we use the material parameters listed in Table I. These are selected to represent an idealized 2 dimensional (2D) layered hybrid organic- inorganic perovskite (HOIP) semiconductor, using parameters based on those measured or calculated for phenethylammonium

TABLE I. Material parameters used for numerical calculations. Parameters are selected to represent an idealized 2D layered hybrid organic- inorganic perovskite semiconductor, using parameters based on those measured or calculated for phenethylammonium lead iodide, PEA_2PbI_4, (PEPI).

Parameter	Value	Description	Source
E_g	2.6 eV	band gap	Ref. [18]
d	0.644 nm	inorganic layer thickness	Ref. [19]
Λ	1.6 nm	layer spacing	Ref. [19]
ε_i	5.4	inorganic layer intrinsic relative dielectric constant	Ref. [20]
ε_o	2.56	organic layer intrinsic relative dielectric constant	Ref. [20]
n_o	1.915	ordinary ray refractive index	Ref. [20]
μ	$0.087m_0$	exciton reduced effective mass	Ref. [18]
m_e	$0.174m_0$	electron in-plane effective mass	Assume $m_e = m_h = 2\mu$
m_h	$0.174m_0$	hole in-plane effective mass	Assume $m_h = m_e = 2\mu$
E_R^e	40 meV	electron Rashba energy	Ref. [21]
α_e	187 meV·nm	electron Rashba coefficient	From E_R^e using Eq. 2
E_R^h	7.6 meV	hole Rashba energy	From α_h using Eq. 2
α_h	-82 meV·nm	hole Rashba coefficient	Ratio of α_h/α_e from Ref. [16]
$w = C\Theta$	12 meV	short-range exchange constant	Ref. [22]
$\sin\theta$	0.277	Crystal field phase angle (Eq. (24))	Ref. [20]
g_e	+2.11	electron out-of-plane g-factor	Ref. [23]
g_h	-0.13	hole out-of-plane g-factor	Ref. [23]
E_p	14 eV	Kane energy for PbI_4 based perovskites	Ref. [11, 12]

lead iodide, PEA_2PbI_4, (PEPI). In our modeling, we neglect vibronic [24] or polaronic [25] structure which creates a complex multiline fine structure in absorption and emission in actual samples of PEPI [24, 26]. For description of quasi-2D structures with inorganic layer thickness d greater than one monolayer (ML) we use the same material parameters as in Table I.

II. LANDAU LEVELS AND INTER-BAND OPTICAL TRANSITIONS IN 2D STRUCTURES WITH LARGE RASHBA SPIN-ORBIT COUPLING

To consider the effect of Rashba terms on the interband transitions in a 2D semiconductor in a magnetic field, we revisit first the theoretical description of the Landau levels for electrons or holes in a simple band 2D system. We take the magnetic field to be in the z direction, $\boldsymbol{B} = B\ \hat{\boldsymbol{z}}$, and model its effects in the Landau gauge, setting the vector potential $\boldsymbol{A} = Bx\hat{\boldsymbol{y}}$, where $\hat{\boldsymbol{y}}$ is a unit vector along the y axis. Without Rashba spin-orbit coupling, the effective mass equation for the motion of an electron or a hole with charge $q = \mp e$, respectively, where e is the elementary charge, in the magnetic field takes the form of a one dimensional harmonic oscillator. Defining the mechanical momentum as $\hat{\boldsymbol{\pi}} = \hbar\hat{\boldsymbol{k}}$, which is related to the canonical momentum $\hat{\boldsymbol{p}}$ through the vector potential by $\hat{\boldsymbol{\pi}} = \hat{\boldsymbol{p}} - q\boldsymbol{A}/c$, we note that $\hat{\pi}_x = \hat{p}_x$; and $\hat{\pi}_y = \hat{p}_y - qBx/c$ from which we find the following critical commutation relation: $[\hat{\pi}_x, \hat{\pi}_y] = [\hat{p}_x, \hat{p}_y] - qB/c\ \ [\hat{p}_x, x] = +i\ \hbar q\ B/c$, where c is speed of light. Crucially, that the sign of commutator depends on the sign of (qB). From this and defining $\hat{\pi}_\pm = \hat{\pi}_x \pm i\hat{\pi}_y$, we arrive at a generalized definition of the magnetic oscillator raising and lowering operators valid for electrons or holes (charge $q = -e$, $+e$ respectively) and either direction of the magnetic field (along $+\hat{\boldsymbol{z}}$ or $-\hat{\boldsymbol{z}}$):

$$\hat{a} = \frac{l_m}{\hbar\sqrt{2}}\left(\hat{\pi}_x + \mathrm{sgn}\left(qB\right) i\hat{\pi}_y\ \right);\ \hat{a}^+ = \frac{l_m}{\hbar\sqrt{2}}\left(\hat{\pi}_x - \mathrm{sgn}\left(qB\right) i\hat{\pi}_y\ \right)\ , \tag{3}$$

where $l_m = \sqrt{c\hbar/|q\ B|}$ is the magnetic length. The spin-independent portion of the Hamiltonian can thus be expressed

$$\hat{H} = \frac{1}{2m}\left\{\hat{p}_x^2 + \ \left(\hat{p}_y - qBx/c\right)^2\right\} = \frac{1}{2m}\hat{\boldsymbol{\pi}}\cdot\hat{\boldsymbol{\pi}} = \hbar\omega_c\ \left(\hat{a}^+\hat{a} + 1/2\right)\ , \tag{4}$$

where $\omega_c = |qB|/mc$ is the cyclotron frequency of the charge carrier written in terms of its effective mass, m. Given the translational invariance in the y direction, we write the envelope function according to the ansatz,

$$\psi_k\left(x, y\right) = \frac{e^{iky}}{\mathcal{N}} f_k\left(x\right)\ , \tag{5}$$

where $\mathcal{N}$ is a normalization factor. Substituting in and solving for the envelope functions, we find that the orbital energies are independent of k and are given in terms of Landau level (LL) quantum number, n by, $E_k\left(n\right) = \hbar\omega_c\left(n + 1/2\right)$, with envelope functions given by,

$$\langle \boldsymbol{r}|k, n\rangle = \psi_{k,n}\left(x, y\right) = \ \frac{e^{iky}}{\mathcal{N}}\mathcal{H}_n\left[x - x_0(k)\right]\exp\left(-\frac{\left[x - x_0(k)\right]^2}{2{l_m}^2}\right)\ . \tag{6}$$

Here $x_0(k)$ is the center of the cyclotron orbit in the x-direction, where,

$$x_0(k) = \hbar kc/qB = \mathrm{sgn}\,(qB)\ \ k\ {l_m}^2, \tag{7}$$

and $\mathcal{H}_n(x)$ is the Hankel polynomial. Inspection of Eq. 6 shows that the magnetic length, l_m, is a measure of the cyclotron orbital radius. The number of degenerate states k in a sample of area A can be shown to be $N = AeB/2\pi\hbar$. [27] Including the Zeeman interaction the Hamiltonian can be written as,

$$\hat{H}(B) = \ \hbar\omega_c \left(\hat{a}^+\hat{a} + \ \frac{1}{2}\right)\hat{I} + \ \frac{g\mu_B B}{2}\hat{\sigma}_z\ . \tag{8}$$

Here, $\hat{I}$ is the 2x2 identity matrix, $\mu_B = e\hbar/(2m_0)$ is the Bohr magneton and g is the Lande g-factor for the carrier.

Rashba term contributions to the Landau level structure of a two-dimensional electron gas in a simple band system were first described by Rashba [7] and Bychkov and Rashba [6]. Here we generalize the analysis to include the Landau level structure of a 2D hole gas in a simple band system, such as are found in 2D hybrid organic-inorganic perovskite semiconductors. With inversion asymmetry in the direction $\hat{\boldsymbol{z}}$ perpendicular to the plane of the 2D system, the Rashba term, Eq. 1 for a given band can be re-cast as,

$$\hat{H}_R = i\ \alpha \left(\hat{k}_-\hat{\sigma}_+ - \hat{k}_+\hat{\sigma}_-\right)\ , \tag{9}$$

where we have defined $\hat{\sigma}_\pm = \frac{1}{2}(\hat{\sigma}_x \pm i\hat{\sigma}_y)$ and $\hat{k}_\pm = \hat{k}_x \pm i\hat{k}_y$, where $\hat{k}_x, \hat{k}_y$ are components of the wave vector operator. The Hamiltonian for a simple band in a magnetic field in the presence of Rashba spin-orbit coupling is thus represented as the 2x2 matrix,

$$\hat{H}(B) = \ \hbar\omega_c \left(\hat{a}^+\hat{a} + \ \frac{1}{2}\right)\begin{bmatrix}1 & 0\\ 0 & 1\end{bmatrix} + \ \frac{g\mu_B B}{2}\begin{bmatrix}1 & 0\\ 0 & -1\end{bmatrix} + \alpha\ \begin{pmatrix}0 & i\hat{k}_-\\ -i\hat{k}_+ & 0\end{pmatrix}\ , \tag{10}$$

which is spanned by the band-edge Bloch functions for the band in question. In the absence of in-plane anisotropy, the conduction band Bloch functions can be represented as the eigenstates of total angular momentum, $J_z = \pm\frac{1}{2}$, which we will denote using double arrows, $|\Uparrow\rangle, |\Downarrow\rangle$, while the valence band Bloch functions can be represented by the spin functions with projection $S_z = \ +1/2\ (-1/2)$, which we will denote as $|\uparrow\rangle, |\downarrow\rangle$. Explicit representations of these states are given in the next section.

To proceed we note that the terms $\hat{k}_\pm$ can be rewritten in terms of raising and lowering operators, Eq. 3. However, critically, for a given direction of $\boldsymbol{B}$, the definition required

depends on the sign of the carrier charge, q. The Rashba Hamiltonian thus takes the conditional form,

$$\hat{H}_R = \begin{cases} \alpha \, \frac{\sqrt{2}}{l_m} \begin{pmatrix} 0 & i\hat{a} \\ -i\hat{a}^+ & 0 \end{pmatrix} & \text{if } (q<0, B>0), \text{or } (q>0, B<0) \ ; \\ \\ \alpha \, \frac{\sqrt{2}}{l_m} \begin{pmatrix} 0 & i\hat{a}^+ \\ -i\hat{a} & 0 \end{pmatrix} & \text{if } (q>0, B>0), \text{or } (q<0, B<0) \ . \end{cases} \tag{11}$$

With either condition we see that the LLs associated with the two angular momentum states are generally mixed. Anticipating solutions associated with two branches, indexed by $\lambda = \pm 1$, we write trial state vectors in the following form: For the conduction electron case ($q < 0$ in positive magnetic field, $B > 0$), the state for LL index n is,

$$|k, n, \lambda\rangle = \begin{cases} = C_{1,\lambda}(n)|n-1\rangle|\Uparrow\rangle + C_{2,\lambda}(n)|k,n\rangle|\Downarrow\rangle, & (n \geq 1, \lambda = \pm 1) \ ; \\ \\ = |k, 0>|\Downarrow\rangle, & (n = 0, \lambda = +1 \text{ only}) \ . \end{cases} \tag{12}$$

This equation also applies for holes, ($q > 0$), in a negative magnetic field, ($B < 0$) if the conduction band basis states $|\Uparrow\rangle, |\Downarrow\rangle$ are replaced by those for the valence band, $|\uparrow\rangle, |\downarrow\rangle$. To distinguish hole LLs from those of the electrons, we will write the hole LLs with index p. For the case of a hole with LL index p in a positive magnetic field $q > 0,\ B > 0$, we write the trial function as,

$$|k, p, \lambda\rangle = \begin{cases} = V_{1,\lambda}(p)|p\rangle|\uparrow\rangle + V_{2,\lambda}(p)|k,p-1\rangle|\downarrow\rangle, & (p \geq 1, \lambda = \pm 1) \ ; \\ \\ = |k, 0>|\uparrow\rangle, & (p = 0, \lambda = +1 \text{ only}) \ . \end{cases} \tag{13}$$

Here again, this equation can also be applied for electrons, ($q < 0$) in a negative magnetic field ($B < 0$) if the basis states $|\uparrow\rangle, |\downarrow\rangle$ for the valence band are replaced with those for the conduction band, $|\Uparrow\rangle, |\Downarrow\rangle$.

It is important to note that the $n = 0$ electron state in Eq. (12) can only exist in the *lower* angular momentum state, $|\Downarrow\rangle$, corresponding to branch $\lambda = +1$; while the $p = 0$ hole state in Eq. (13) can only exist in the *upper* spin state, $|\uparrow\rangle$, corresponding to branch $\lambda = +1$. We note that these $n = 0$ and $p = 0$ states are *unaffected* by Rashba splitting.

The energy of the nth Landau level $E^{\lambda}_{e,h}(n) = \hbar\omega_{e,h}\varepsilon^{\lambda}_{e,h}(n)$ in a positive magnetic field is then found to be proportional to the cyclotron energy of the electrons or hole, $\omega_{e,h}$ respectively. The dimensionless energy term $\varepsilon^{\lambda}_{e,h}(n)$ is given for elecrons (e) and holes (h) by,

$$\varepsilon^{\lambda}_{e,h}(n) = \begin{cases} \delta_{e,h}, \ n = 0, \ \lambda = +1 \\ n + \lambda\sqrt{\delta^2_{e,h} + n\gamma^2_{e,h}}, \ n \geq 1 \end{cases} \tag{14}$$

where the term $\delta_{e,h}$ depends on the sign of the carrier charge and of the magnetic field:

$$\delta_{e,h} = \frac{1}{2}\left(1 + \mathrm{sgn}(qB)\frac{m_{e,h}g_{e,h}}{2m_0}\right) \ . \tag{15}$$

In these expressions, $g_{e,h}$ are the electron or hole g-factors, while $\gamma_{e,h} = 2\sqrt{E^{e,h}_R/\hbar\omega_{e,h}}$ where Rashba energy $E^{e,h}_R$ is defined in Eq. (2). The corresponding wavefunctions in Eq. 12 were determined for electrons in a positive magnetic field by Rashba [7]. For the LL with $n = 0$

$$C_{1,+1}(0) = 0, \quad C_{2,+1}(0) = 1, \tag{16}$$

for $n \geq \ 1$ the wave function can be written as:

$$C_{1,\lambda}(n) = \frac{i\,\mathrm{sgn}(\alpha)\lambda}{\sqrt{2}}\sqrt{1 - \frac{\lambda\delta_e}{\sqrt{\delta^2_e + n\gamma^2_e}}}, \ C_{2,\lambda}(n) = \frac{1}{\sqrt{2}}\sqrt{1 + \frac{\lambda\delta_e}{\sqrt{\delta^2_e + n\gamma^2_e}}} \ . \tag{17}$$

The corresponding solutions for holes with $p = 0$ are given by,

$$V_{1,+1}(0) = 1, \quad V_{2,+1}(0) = 0 \ , \tag{18}$$

and for $p \geq \ 1$ can be written as:

$$V_{1,\lambda}(p) = \frac{i\,\mathrm{sgn}(\alpha)\lambda}{\sqrt{2}}\sqrt{1 + \frac{\lambda\delta_h}{\sqrt{\delta^2_h + p\gamma^2_h}}}, \ V_{2,\lambda}(p) = \frac{1}{\sqrt{2}}\sqrt{1 - \frac{\lambda\delta_h}{\sqrt{\delta^2_h + p\gamma^2_h}}}, \tag{19}$$

The magnetic field dependence of the Landau levels are shown in Fig.2. For illustration purposes, in Fig.2, the electron Rashba coefficient is non-zero while the hole Rashba coefficient is set to zero. On the same figure we show the interband selection rules, developed in the next section, for optical transitions with normally incident circularly polarized light $\hat{\sigma}^{\pm}$, which require $n = p \pm 1$, where n and p denote the LL numbers of the electron and hole states, respectively. These selection rules and Eq. (14) describing the magnetic field dependencies of the electron and hole Landau levels allows description of the absorption spectra of 2D layers. Consequently if the multiple interband optical transitions between

Landau levels are observed, comparison of the experimental magnetic field dependence with theory allows extraction of the Rashba parameter of the conduction and valence bands.

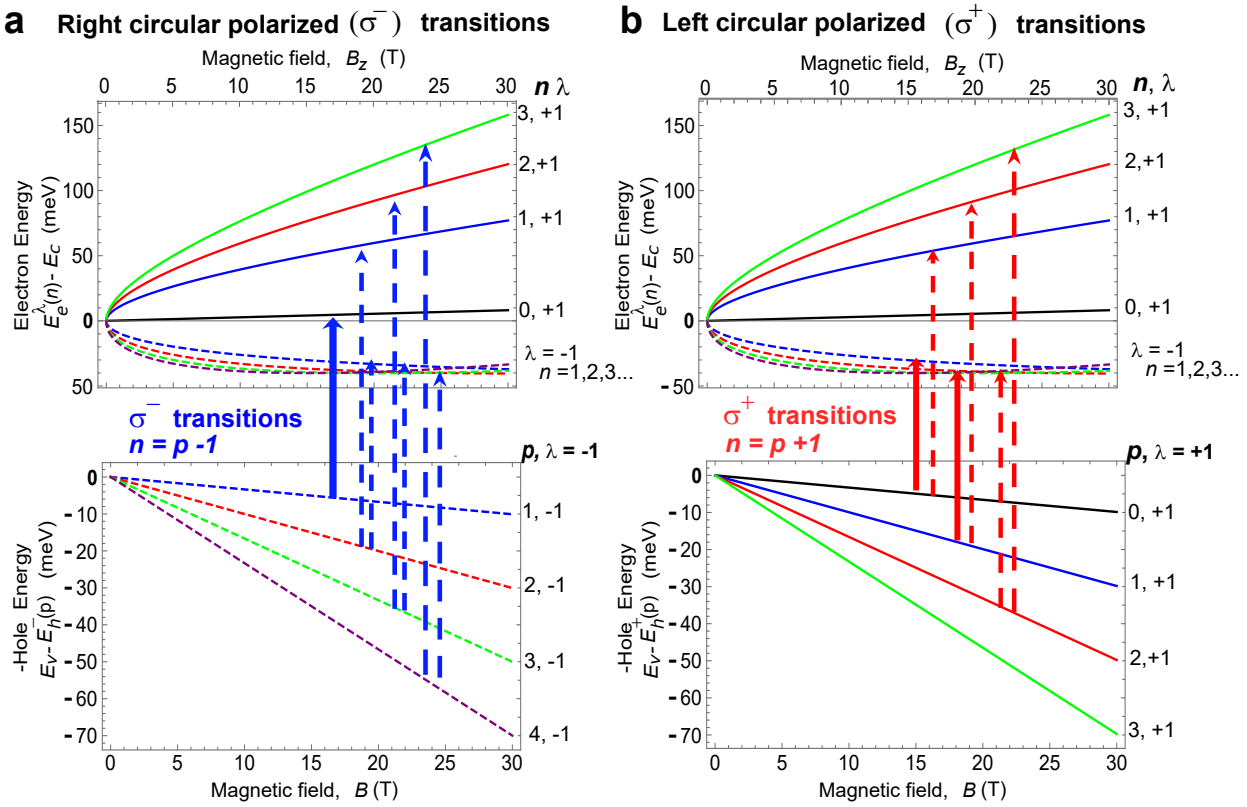

FIG. 2. Magnetic field dependence of the lowest electron and hole Landau levels calculated using equal electron and hole effective masses $m_e = m_h = 0.174m_0$, with the electron and hole g-factors [23] listed in Table I. The calculation is performed with large Rashba splitting in the conduction band, $\alpha^e = 187$ meV·nm, while for clarity, the Rashba splitting in the valence band is set to zero, $\alpha^h = 0$. The arrows in panels **a** and **b** depict the optical transitions to a given electron Landau level, n, λ, from the valence band state corresponding to hole level, p, λ. For circularly polarized light $\hat{\sigma}^{\pm}$, these require $n = p \pm 1$, independent of the level branch indices λ. The optical transitions that cause giant MCD at the band edge are marked by solid arrows in panels **a** and **b**; these transition correspond to the circled transitions in Fig.3 panel **a**. Levels with $n, p = 0, 1, 2, 3$ are colored black, blue, red, green, respectively.

III. ABSORPTION AND MAGNETIC CIRCULAR DICHROISM

To describe interband absorption and MCD in perovskites in the presence of Rashba splitting, we must find the optical selection rules for circularly polarized light in Faraday geometry and evaluate the polarization dependent transition oscillator strength. We assume that light is incident in the positive $\hat{z}$ direction, normal to the perovskite layers. The light polarization vector is given for left and right circularly polarized light by the polarization vectors, $\hat{\sigma}^+$ and $\hat{\sigma}^-$, respectively, where,

$$\hat{\sigma}^{\pm} = 1/\sqrt{2}(\hat{x} \pm i\hat{y}) \ . \tag{20}$$

Since the interaction Hamiltonian is proportional to $e/c\boldsymbol{A}\cdot\hat{\boldsymbol{p}}$, where $\boldsymbol{A}$ is the vector potential of the light and $\hat{\boldsymbol{p}}$ is the dipole operator, we find the transition dipole matrix element connecting the initial state, the crystal ground state, $|G\rangle$ where $\langle r_e, r_h|G\rangle \ = \delta(\ r_e - r_h)$, and a given electron-hole pair state. We write the e/h pair state for a given magnetic field, B, as, $|\mathcal{P}_{\{j\}}\rangle \equiv |k^e, n, \lambda_e; k^h, p, \lambda_h\rangle \ = |k^e, n, \lambda_e\rangle|k^h, p, \lambda_h\rangle$, where the term $\{j\}$ denotes the set of quantum numbers specifying the electron and hole states within the pair, and evaluate the matrix element by time reversing the hole wave function and moving it from the bra to the ket position in the usual manner:[28]

$$\langle\mathcal{P}_{\{j\}}|\hat{\boldsymbol{p}}|G\rangle = \langle k^e, n, \lambda_e|\hat{\boldsymbol{p}}\left\{T|k^h, p, \lambda_p\rangle\right\} \ . \tag{21}$$

Here, T is the time reversal operator, $T = \ -i\ \sigma_y\ \mathcal{K}$, where $\mathcal{K}$ is the conjugation operator operating on the orbital functions and σ_y is the Pauli matrix which flips the spin.

To proceed further we need the explicit representations of the band edge Bloch functions. For the valence band, the Bloch functions are eigenstates of the projection of spin angular momentum on the z axis,

$$|\uparrow\rangle \ = S\ \uparrow, \qquad |\downarrow\rangle \ = S\ \downarrow \tag{22}$$

Here, the symbol S denotes an orbital function that transforms as an invariant under the operations of the crystal point symmetry group, while $\uparrow$ ($\downarrow$) denote the spin functions with projection $S_z = \ +1/2\ (-1/2)$. For the conduction band, neglecting in-plane anisotropy, the conduction band Bloch functions have $J_z = \pm\frac{1}{2}$, which we denote using double arrows: $\Uparrow, \Downarrow$.

These are represented by, [13, 14, 20, 22, 29]

$$
\begin{aligned}
|\Uparrow\rangle &= -\left\{\sin\theta Z\uparrow + \cos\theta\frac{(X+i\ Y)}{\sqrt{2}}\downarrow\right\}\ , \\
|\Downarrow\rangle &= \left\{-\cos\theta\frac{(X-i\ Y)}{\sqrt{2}}\uparrow + \ \sin\theta Z\downarrow\right\}\ .
\end{aligned}
\tag{23}
$$

In this expression the symbols $X,\ Y,\ Z$ denote orbital functions that transform like x, y, z under the operations of the point group. The phase angle θ determines the mixing of the lowest $J = 1/2$ conduction bands and the upper $J = 3/2$ conduction bands and is determined by the magnitude of spin orbit splitting, Δ_{SO}, and the crystal field splitting, δ, of the conduction band:[13, 14, 20, 22, 29]

$$
\tan 2\theta = \frac{2\sqrt{2}\Delta_{\rm SO}}{\Delta_{\rm SO} - 3\delta} \qquad\qquad 0 \le \theta \le \frac{\pi}{2}\ . \tag{24}
$$

With these definitions it is straightforward to evaluate the oscillator strength for absorption of left and right circularly polarized light, $\hat{\sigma}^{\pm}$ for a given magnetic field, B. We recall the definition of oscillator strength,

$$
f^{\pm}_{\{j\}} = \frac{2|P^{\pm}_{\{j\}}|^2}{m_0 E_{\{j\}}}\ , \tag{25}
$$

where $E_{\{j\}}$ is the energy of the given optical transition creating the state $\{j\}$ by absorption from the crystal ground state G. To write the oscillator strength we need to evaluate the squared magnitude of the transition dipole matrix elements that create a given electron-hole pair state $\{j\}$. These matrix elements are readily evaluated:

$$
\begin{aligned}
|P^{+}_{\{j\}}|^2 &= |\hat{\sigma}^{+}\cdot\langle k^e, n, \lambda_e; k^h, p, \lambda_h|\hat{\boldsymbol{p}}|G\rangle^2 = |P|^2\cos^2\theta\,|C_{1,\lambda_e}(n)V_{1,\lambda_h}(p)|^2\,\delta_{n,p+1}\delta_{k^e,-k^h}\ , \\
|P^{-}_{\{j\}}|^2 &= |\hat{\sigma}^{-}\cdot\langle k^e, n, \lambda_e; k^h, p, \lambda_h|\hat{\boldsymbol{p}}|G\rangle^2 = |P|^2\cos^2\theta\,|C_{2,\lambda_e}(n)V_{2,\lambda_h}(p)|^2\,\delta_{n,p-1}\delta_{k^e,-k^h}\ ,
\end{aligned}
\tag{26}
$$

In these expressions, $P = -\ i\ \langle S|\hat{\boldsymbol{p}}|X\rangle = -i\langle S|\hat{\boldsymbol{p}}|Y\rangle$ is the Kane momentum matrix element [30], related to the Kane energy E_p by, $E_p = 2|P|^2/m_0$. The Kronecker delta function $\delta_{k^e,-k^h}$ is a reflection of the momentum conservation: $k^h\ +\ k^e\ =\ 0$, which implies, via Eq. (7), that electron and hole LLs have allowed transitions only from the same orbital center. The Kronecker delta function $\delta_{n,p\pm1}$ gives the LL number selection rule for $\hat{\sigma}^{\pm}$ polarized light: $n = p \pm 1$ irrespective of the branch indices λ_e, λ_h in the general case.

In the special case that there is no Rashba splitting in either band, both the electron and the hole states are pure angular momentum states. Consequently, for this case there is

an additional branch selection rule, namely, that only cross-branch transitions are allowed: For absorption of $\hat{\sigma}^{\pm}$ polarized light, the allowed transitions are those that obey $\lambda_h \to -\lambda_e$. This leads to ordinary MCD reflecting the expected Zeeman splitting between transitions allowed for $\hat{\sigma}^{\pm}$ polarized light, with energy separation $\Delta E_{zee} = \mu_B(g_e + g_h)B$. This case is illustrated for example in Ref. [31].

In the special case that there is significant Rashba splitting only in the conduction band and vanishing Rashba splitting in the valence band (not unreasonable since in the valence band, the Rashba coefficient is expected to be much smaller than in the conduction band [16]), the valence band LLs are pure spin states (see Eqs. (13) and (17)). This results in the following modifications of the selection rules: For $\hat{\sigma}^{+}$ polarized light the allowed transition only occurs from the valence band level p with branch $\lambda_h = +1$ to electron state $n = p + 1$ of either the upper or lower branch, $\lambda_e = \pm 1$; while for $\hat{\sigma}^{-}$ polarized light the allowed transitions occurs from the hole level p with branch $\lambda_h = -1$ to the electron level $n = p - 1$ of either the upper or lower branch, $\lambda_e = \pm 1$. These selection rules are illustrated in Fig.2. One can see from Fig.2 that due to the special selection rules connected with the $n = 0$ Landau level in the presence of Rashba terms, the transition terminating at $n = 0$ is 100% polarized for σ^{-} light (this transition is marked by a bold solid blue arrow) while the two lowest energy transitions (shown by solid red arrows) are σ^{+} polarized. Since the Rashba splitting causes all other levels with $n \geq 1$ to be well separated in energy from the pure angular momentum state $n = 0$, we expect this feature to result in a giant MCD signal.

With the oscillator strength in hand we can determine the energy-dependent absorption coefficient $\alpha^{\pm}(E; B)$ for a given magnetic field, B. This entails a sum over the final electron and hole Landau level pair states, $\{j\}$. In CGS units this is given by,[32]

$$\alpha^{\pm}(E) = \frac{2\pi^2\hbar e^2}{m_0} \frac{1}{nc\Lambda} \frac{1}{A} \sum_j f^{\pm}_{\{j\}}\, g\left(E - E_{\{j\}}\right) \ , \tag{27}$$

where n is the refractive index, c is the speed of light, Λ is the period of the 2D perovskite, A is the area of the sample, and $g(E - E_{\{j\}})$ is the normalized absorption lineshape function for the transition terminating on the state $\{j\}$. For all the calculations we will present, this is assumed to be a Gaussian,

$$g(E - E_{\{j\}}) = \frac{1}{\sqrt{2\pi}\sigma} e^{-\frac{(E-E_{\{j\}})^2}{2\sigma^2}} \ , \tag{28}$$

where the full-width at half maximum linewidth $\Gamma = 2\sqrt{2\ln 2}\sigma$.

Let us decompose the expression for the absorption coefficient further. The matrix element in Eq. (25) can be reduced using Eq. (26), resulting in the absorption for $\hat{\sigma}^+$ polarized light given by,

$$\alpha^+(E;B) = \frac{2\pi^2\hbar e^2}{m_0}\frac{1}{nc\Lambda}\frac{1}{A}\frac{E_p}{E_g}\cos^2\theta\sum_{k_e}\sum_{n,\lambda_e,\lambda_h}|C_{1,\lambda_e}(n)V_{1,\lambda_h}(n-1)|^2\ g\left(E-E_{\lambda_e}(n)-E_{\lambda_h}(n-1)\right)\ , \tag{29}$$

and the absorption for $\hat{\sigma}^-$ polarized light given by,

$$\alpha^-(E;B) = \frac{2\pi^2\hbar e^2}{m_0}\frac{1}{nc\Lambda}\frac{1}{A}\frac{E_p}{E_g}\cos^2\theta\sum_{k_e}\sum_{n,\lambda_e,\lambda_h}|C_{2,\lambda_e}(n)V_{2,\lambda_h}(n+1)|^2\ g\left(E-E_{\lambda_e}(n)-E_{\lambda_h}(n+1)\right)\ . \tag{30}$$

Here we have approximated $E_{\{j\}} \approx E_g$ in the denominator to pull it out of the sum. We see that these expressions each involve a sum over k_e of a sum which is independent of k_e; we can therefore eliminate the sum over k_e. As noted in the last section, the number of distinct states k_e in a sample of area A can be shown to be, $N = AeB/2\pi\hbar$ [27]. This is simply the ratio of the sample area to the square of the magnetic length, $N = A/2\pi l_B^2$. Therefore the term A cancels out of the expressions above. A final refinement is to include the effect of electron-hole Coulomb interactions via the Sommerfeld Coulomb enhancement factor for 2D interband transitions. In terms of the exciton binding energy, $B_x = |E_{10}|$, which is of order ~ 300 meV for single layer perovskites (see Appendix A), this factor is given by, [33, 34],

$$S_{2D}(E) = \frac{2}{\exp\left(-2\pi\sqrt{\frac{B_x}{E-E_g}}\right)+1} \sim 2, \qquad (E-E_g \ll B_x)\ , \tag{31}$$

which takes the approximate value 2 within B_x of the band edge. Putting all these terms together we have,

$$\begin{aligned}
\alpha^+(E;B) &= S_{2D}\frac{2\pi^2\hbar e^2}{m_0}\frac{1}{nc\Lambda}\frac{E_p}{E_g}\cos^2\theta\frac{eB}{2\pi\hbar}\sum_{n,\lambda_e,\lambda_h}|C_{1,\lambda_e}(n)V_{1,\lambda_h}(n-1)|^2\ g\left(E-E_{\lambda_e}(n)-E_{\lambda_h}(n-1)\right)\ , \\
\alpha^-(E;B) &= S_{2D}\frac{2\pi^2\hbar e^2}{m_0}\frac{1}{nc\Lambda}\frac{E_p}{E_g}\cos^2\theta\frac{eB}{2\pi\hbar}\sum_{n,\lambda_e,\lambda_h}|C_{2,\lambda_e}(n)V_{2,\lambda_h}(n+1)|^2\ g\left(E-E_{\lambda_e}(n)-E_{\lambda_h}(n+1)\right)\ .
\end{aligned} \tag{32}$$

These functions are then used to evaluate the MCD using,

$$\text{MCD} \equiv \Delta A = A^+ - A^-\ . \tag{33}$$

Here, $A^\pm$ is the decadic absorbance for $\hat{\sigma}^\pm$ polarized light given by, $A^\pm = -\log_{10}(e^{-\alpha^\pm L}) = \alpha^\pm L/\ln 10$, where L is the sample thickness and $\alpha^\pm$ are the absorption coefficients for $\hat{\sigma}^\pm$ polarized light.

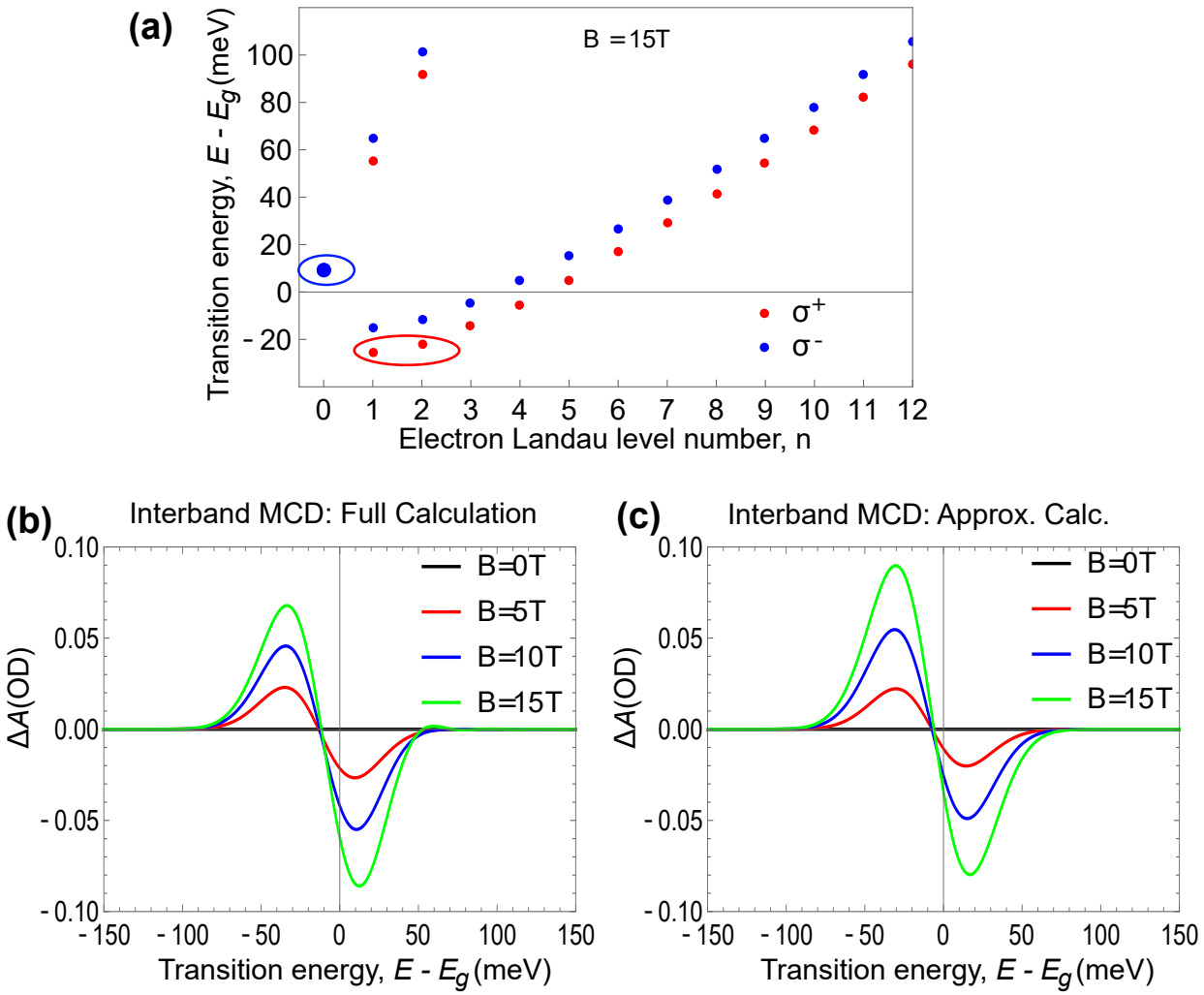

FIG. 3. Interband optical transitions and MCD stimulated by absorption of σ^+ and σ^- polarized light in a system with Rashba splitting only in the conduction band with $\alpha^e = 187$ meV·nm. Panel **a**: Energy dependence of the transitions to the electron Landau level, n, calculated in magnetic field $B = 15$ T. Transitions polarized σ^- are shown in blue dots while those polarized σ^+ are shown with red dots. The size of the dot corresponds roughly to the relative transition oscillator strength. The MCD, ΔA, in units of optical density (OD) is calculated as the difference of the decadic absorbance of σ^+ and σ^- polarized light in magnetic fields 5, 10 and 15 T, taking into account all Landau levels transitions within the plotted energy range, panel **b**, and calculated using only the circled transitions (see text) panel **c**. The absorbance and MCD calculations assume a sample thickness $L = 100$ nm with material parameters given in Table I. Each transition is taken to have a normalized Gaussian lineshape with full width at half-maximum $\Gamma = 50$ meV.

In Fig. 3 we show calculations of the MCD corresponding to the case depicted in Fig. 2, where we assumed that large non-zero Rashba splitting occurs in the conduction band with no Rashba splitting in the valence band. As noted above, due to the special selection rules connected with the $n = 0$ electron Landau level in the presence of Rashba terms, the transition terminating at $n = 0$ is 100% polarized for σ^- light. This transition, shown with the solid blue arrow in Fig. 2 **a**, is circled in blue in Fig 3 panel **a**. At the same time, the two lowest energy transitions, circled in red in the same panel, (shown with the solid red arrows in Fig. 2 **b**) are σ^+ polarized; each of these transitions has roughly half the oscillator strength as the transition terminating on the $n = 0$ electron LL. Since all other levels are well separated in energy from the σ^- polarized transition terminating in the $n = 0$ level, and are nearly degenerate with roughly equal oscillator strengths, the net result is a giant MCD signal with a derivative-like line shape. Panel **b** of Fig 3 shows the full MCD calculation confirming that this is the case. In panel **c** we show an approximated calculation including only the transitions circled in panel **a**, which closely matches the result of the full calculation, confirming our analysis.

It is instructive to compare this result to two model cases: First, the MCD that would be expected for free carrier transitions in the absence of Rashba splitting; and second, the MCD expected for excitonic transitions.

For free carrier transitions, assuming parabolic band dispersion, and assuming that each free carrier transition is Gaussian broadened according to Eq. (28), the absorbance A_{fc} for a sample of thickness L can be shown to be given by,

$$A_{fc}\,(E) \approx \frac{L}{\ln 10}\; S_{2D}\frac{2\pi^2\hbar e^2}{m_0}\;\frac{1}{nc\Lambda}\frac{\mu}{2\pi\hbar^2}\frac{E_p}{E_g}\cos^2\theta\;\;\frac{1}{2}\;\left(1+\mathrm{erf}\left(\frac{\mathrm{E}-\mathrm{E_g}}{\sqrt{2}\sigma}\right)\right)\;. \qquad (34)$$

Here, the factor $\mu/2\pi\hbar^2$ represents the joint density of states per unit area per unit transition energy for k-conserving transitions between the valence and conduction bands. As before, $\mu = (1/m_e + 1/m_h)^{-1}$. Using this expression, in the limit that the linewidth $\Gamma \gg \hbar\omega_e$, MCD associated with the free carrier interband transitions without Rashba splitting occurs at the band edge due to the Zeeman shift of the carrier levels. The MCD is proportional to the derivative of the absorbance at the band edge and thus has a Gaussian line-shape:

$$\begin{aligned}\Delta A_{fc}(B) &= -\frac{dA_{fc}}{dE}g_{fc}\mu_B B \\ &= \frac{L}{\ln 10}\; S_{2D}\frac{2\pi^2\hbar e^2}{m_0}\;\frac{1}{nc\Lambda}\frac{\mu}{2\pi\hbar^2}\frac{E_p}{E_g}\cos^2\theta\; g(E-E_g)\; g_{fc}\mu_B B\;, \end{aligned} \qquad (35)$$

where $g_{fc} = g_e + g_h$ is the interband g-factor for Faraday configuration. This result stands in distinct contrast to what we found above and in Fig. 3 for the case of Rashba splitting in the conduction band, where the MCD has a derivative-like signature.

In the second case of interest, the absorbance A_{exc} due to bound exciton transitions can be written similarly to Eq.(27) in terms of the exciton oscillator strength per unit area, $f_{n,0}/A$ for each 2D exciton state with principle quantum number $n \geq 1$ and azimuthal quantum number 0. These are given in Appendix A (see Eq. (A9)). The resulting expression for the absorbance can be written,

$$A_{exc}\,(E) = \frac{L}{\ln 10}\frac{2\pi^2\hbar e^2}{m_0}\,\frac{1}{nc\Lambda}\sum_n \left(\frac{f_{n,0}}{A}\right)\; g\,(E - E_{n,0})\;\;, \tag{36}$$

where as before we assume that the transitions are broadened by Gaussian lineshape functions (Eq.(28)). Each bound exciton transition exhibits MCD due to the Zeeman splitting of the levels. The MCD can be computed from the derivative of the absorbance:

$$\Delta A_{exc}(B) = -\frac{dA_{exc}}{dE}\; g_{exc}\; \mu_B\; B\;, \tag{37}$$

where $g_{exc} = g_e + g_h$ denotes the exciton g-factor for Faraday configuration [11, 12] for the fine structure levels with angular momentum $J_z = \pm 1$. Notably, the MCD of the excitons that can be measured in absorbance in Faraday geometry is independent of the prescence or absence of Rashba terms, since the $J_z = \pm 1$ fine structure levels are not affected by the Rashba splitting [13, 14, 29] (see discussion in Appendix B). Unlike the free carrier band edge transitions, the exciton MCD signature is derivative- like in contrast to what we found for the band edge free carrier transitions in the absence of Rashba splitting, but similar in this respect to the case of Rashba splitting in the conduction band, where the MCD also has a distinct derivative like signature. How can we distinguish between the derivative like signatures of bound exciton transitions and those associated with Rashba splitting?

We address this question in Figure 4. The figure shows, in the top row of panels, the polarization-averaged absorbance calculated in zero magnetic field including the 1S and 2S levels of bound exciton and the interband transitions, and in the second row of panels, the MCD calculated at magnetic fields $B = 0, 5, 10,$ and 15 T, using the parameters listed in Table I. The polarization averaged absorbance spectra at magnetic fields up to 15T are visually not significantly different from the spectra at B=0 so only the zero field spectra are shown. Panels **a** and **b** show the absorbance and MCD with no Rashba effect in either the conduction

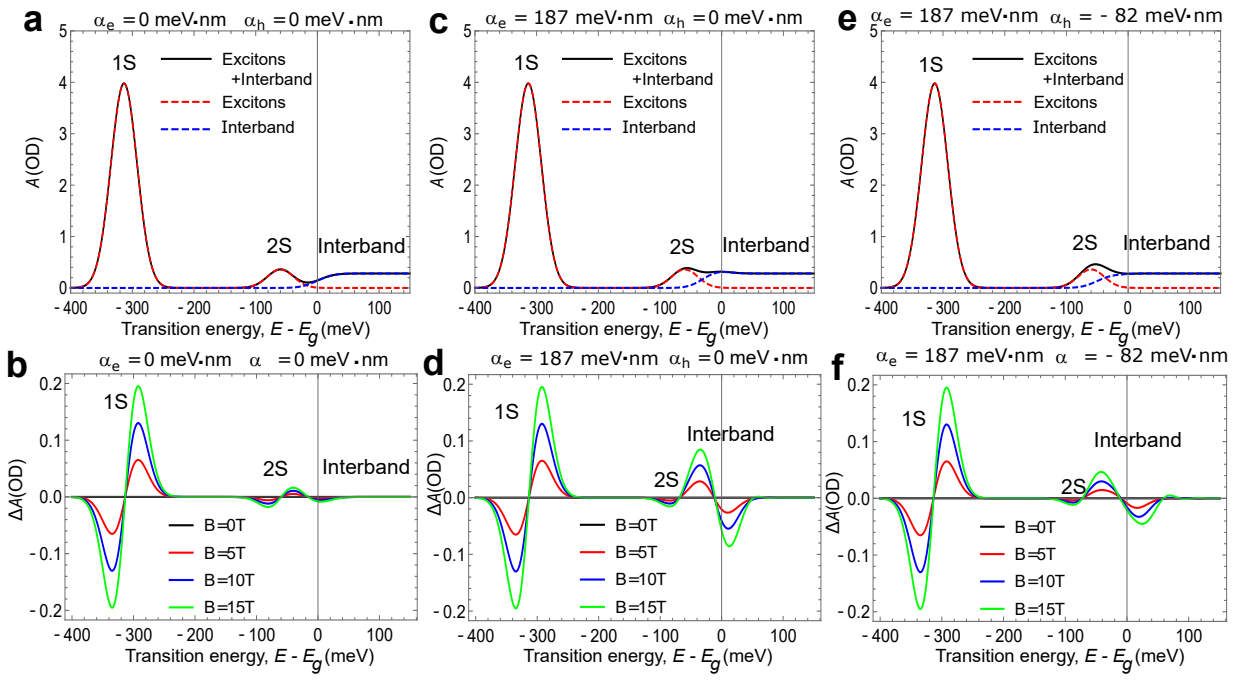

FIG. 4. Interband absorption and magnetic circular dichroism (MCD) including exciton effects, with and without Rashba splitting. The absorbance and MCD in units of optical density (OD) are calculated in the absence of Rashba terms, panel **a** and **b**, respectively; for Rashba coefficients $\alpha^e = 187$ meV·nm and $\alpha^h = 0$, panels **c** and **d**; and for $\alpha^e = 187$ meV·nm and $\alpha^h = -82$ meV·nm, panels **e** and **f**. In all three cases, the absorbance due to the of the 1S and 2S exciton transitions are included. Calculations in panels **b,d,f** are conducted for the magnetic fields $B = 0, 5, 10,$ and 15 T. The calculations assume a sample thickness $L = 100$ nm with material parameters given in Tables I and A1. Each transition is taken to have a normalized Gaussian lineshape with full width at half-maximum $\Gamma = 50$ meV.

or valence bands; panels **c** and **d** show the absorbance and MCD with Rashba splitting in the conduction band only, while panels **e** and **f** show results calculated with Rashba splitting in both the conduction and valence bands. The dominant MCD signals in panel **b**, calculated with no Rashba splitting, are the derivative-like signatures associated with the 1S and 2S exciton transitions. For this case the unipolar band edge feature associated with the free carrier transitions is very weak. By contrast, panel **d**, corresponding to the case of large Rashba splitting in the conduction band, has a dominant derivative-like MCD lineshape associated with the near-band-edge transitions involving the $n = 0, 1, 2$ electron LLs (see

Fig. 3), but the MCD has opposite polarity to that of the 1S and 2S exciton features. This is a characteristic tell-tale for the existence of Rashba splitting. The last case, with Rashba splitting in both the conduction and valence bands, shown in panel **f**, is qualitatively similar to that with Rashba splitting only in the conduction band but with somewhat reduced magnitude of the MCD.

To quantify the relative MCD values for different transitions and /or different models, it is useful to plot the absolute value of the MCD, normalized to the absorbance at the position of the maximum MCD value, versus magnetic field. This is shown in Fig. 5 for the 1S and 2S exciton transitions and for the interband transitions for each model shown in Fig. 4. For cases where the MCD is derivative-like, we select the absolute value of the MCD at the lower energy lobe of the MCD lineshape. Inspection of Fig. 5 shows immediately that the normalized MCD for the interband transitions with Rashba splitting are much larger than for the excitonic features or for the free carrier model without Rashba splitting. To quantify this further, for each of the models shown in Fig.5 we can define an effective g-factor, g_{eff}, defined as,

$$g_{eff} \equiv \frac{1}{\mu_B} \left| \frac{(\partial |\Delta A|_{max}/\partial B)}{(\partial A/\partial E)_{E_{max}}} \right| \ . \tag{38}$$

For reference, we note that the input model g-factor for the excitons and the free carrier transitions in the absence of Rashba splitting is $g_{exc} = g_{fc} = g_e + g_h = 1.98$ (see Table I). Unsurprisingly, the effective g-factors for the exciton 1S and 2S transitions calculated using Eq. (38) matches this value exactly: $g_{eff} = 1.98$. For the band-edge free carrier absorption in the absence of Rashba splitting, the effective g factor is slightly larger at $g_{eff} = 2.03$, reflecting a slight impact of the emergence of Landau levels at the higher magnetic fields in the calculated range, not accounted for in the simple model reflected in Eq. 34 which is only valid for $\Gamma \gg \hbar\omega_e$. By contrast, in the presence of Rashba splitting in the conduction band alone, with Rashba coefficient $\alpha^e = 187$ meV·nm, the effective g-factor determined using Eq. (38) is much higher, $g_{eff} = 11.3$. With Rashba splitting in both the conduction and valence bands, with Rashba coefficients $\alpha^e = 187$ meV·nm and $\alpha^h = -82$ meV·nm, the result is, $g_{eff} = 8.4$. This giant MCD, reflected in the greatly enhanced effective g-factors, plus the derivative like line-shape and polarity reversal relative to the true Zeeman-driven MCD of the exciton lines, serve as signatures of the presence of Rashba splitting according to the Rashba invariant, Eq. 1.

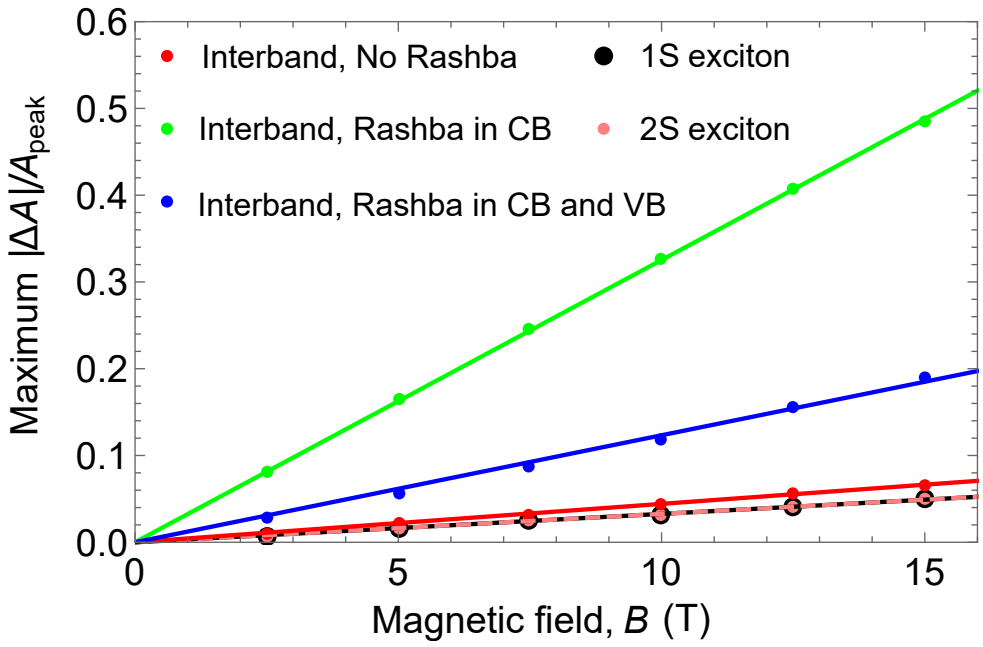

FIG. 5. Comparison of the magnitude of the absorbance normalized MCD calculated for different models. For each model, the plot shows the absolute value of the MCD ($|\Delta A|$)normalized to the polarization averaged absorbance at the position of maximum MCD (A_{peak}). For cases where the MCD is derivative-like we select the absolute value of the MCD at the lower energy lobe of the MCD lineshape. The 1S and 2S exciton models are shown by black and pink circles respectively. The model accounting for inter-band optical transitions with no Rashba effect are shown with red circles; the inter-band transition model with Rashba splitting in the conduction band only is shown with green circles, while the inter-band transition model with Rashba splitting in both the conduction and valence bands is shown with blue circles. The calculations assume a sample thickness $L = 100$ nm with material parameters given in Table I. Each transition is taken to have a normalized Gaussian lineshape with full width at half-maximum $\Gamma = 50$ meV.

IV. DIAMAGNETIC SHIFT OF THE EXCITON LINES

The diamagnetic shift of the exciton at $K = 0$ exciton line is commonly obtained after averaging the diamagnetic term in the exciton Hamiltonian [35], $e^2B^2\rho^2/8\mu$, where $\rho^2 = x^2 + y^2$ and B is the magnitude of the magnetic field normal to the 2D semiconductor layers.

The corresponding shift can be written as

$$\Delta E_d^0 = CB^2 \tag{39}$$

where C for 1S and 2S optically active 2D excitons can be written as

$$C_{1,0} = \frac{e^2}{8\mu}\langle 1,0|\rho^2|1,0\rangle = \frac{e^2}{8\mu}\frac{3a_{1,0}^2}{8}\ , C_{2,0} = \frac{e^2}{8\mu}\langle 2,0|\rho^2|2,0\rangle = \frac{e^2}{8\mu}\frac{117a_{2,0}^2}{8}\ , \tag{40}$$

where μ is the reduced mass of the exciton, $|1,0\rangle$ and $|2,0\rangle$ denote the 1S and 2S exciton states, and $a_{1,0}$, $a_{2,0}$ are the radii of the 1S and 2S exciton wavefunctions described in Eqs.(A5)-(A6).

The separation of variables for an exciton in an external magnetic field, $\boldsymbol{B}$, is not a trivial problem. The problem was first solved by Gor'kov and Dzyaloshinskii [35] who showed that this procedure results in the mixing of the electron/hole relative coordinate $\boldsymbol{r}$ and the exciton center of mass motion momentum $\hbar\boldsymbol{K}$:

$$\hat{H}_{mix} = \frac{e\hbar}{Mc}(\boldsymbol{K}\times\boldsymbol{B})\cdot\boldsymbol{r}\ , \tag{41}$$

where M is the mass of the exciton center of mass motion, c is the speed of light, and e is the electron charge. Equation (41) shows that diamagnetic shift of the exciton with some non-zero momentum $\boldsymbol{K}$ decreases with increase in $\boldsymbol{K}$. This happens because the mixing term $\hat{H}_{mix}$ leads to second order corrections to the ground exciton level, which are proportional to B^2 and are always negative. In the case of 2D excitons this correction can be estimated as:

$$\Delta E_d(K) = -\left(\frac{e\hbar BK}{Mc}\right)^2 \sum_{m=\pm 1}\frac{\langle 1,0|\boldsymbol{r}|2,m\rangle^2}{|E_{1,0}-E_{2,m}|}\ , \tag{42}$$

where $E_{1,0}$ and $E_{2,\pm 1}$ are the energies of the 1S and 2P two-dimensional excitons relative to the band gap, and the matrix element $\langle 1,0|\boldsymbol{r}|2,\pm 1\rangle$ is taken between the eigenfunctions $|1,0\rangle$ and $|2,\pm 1\rangle$ of the 1S and 2P states respectively. Equation (42) shows that there is a negative correction proportional to B^2 and K^2.

In the case of the Rashba exciton, the exciton dispersion has a minimum at some K_R (see Fig. 1) whose magnitude is controlled by the Rashba coefficients of the conduction and valence bands and the electron and hole effective masses. The exciton emission can occur via this minimum. The binding energy of the ground exciton decreases with 2D perovskite thickness while exciton radius increases. As a result the decrease of the diamagnetic shift

connected with the mixing $\hat{H}_{mix}$ increases in thicker 2D perovskite layers, if we neglect the modification of the Rashba coefficient.

The momentum-dependent correction to the diamagnetic shift coming from Eq (42) can be written for the 1S exciton as $\Delta E_d(K_R) = G_{10}B^2$ where,

$$G_{1,0} = -\,2\left(\frac{2\mu_B K_R\,|\langle 1,0|x|2,1\rangle|}{M/m_0}\right)^2 \frac{1}{|E_{1,0}-E_{2,1}|}\,. \tag{43}$$

Here, μ_B is the Bohr magneton, K_R is the Rashba k-vector minimum, M is the total exciton mass, and m_0 is the free electron mass. The factor of 2 comes from the sum over m in Eq. (42). We see that G_{10} is always negative.

In principle the quantitative analysis of this shift allows extraction of K_R. Consequently if we know the carrier effective masses we can determine the Rashba coefficients. It is useful to plot the diamagnetic coefficients versus the thickness of the inorganic layer in monolayers of lead-halide octahedra. This is shown in Fig. 6 using the material parameters listed in

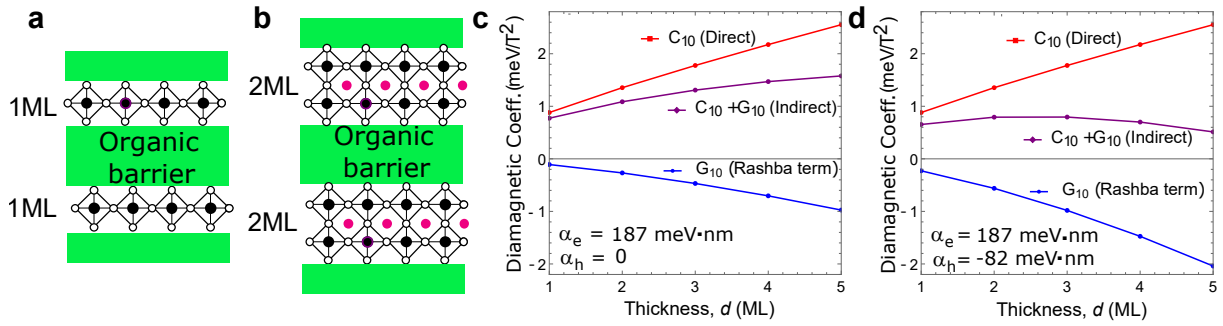

FIG. 6. The dependence of the diamagnetic coefficients that describe the diamagnetic shift of the 1S exciton line versus inorganic layer thickness, d in monolayers (ML). Panels **a** and **b** are cartoons showing 2D perovskites with 1 and 2 ML thickness, respectively. The shift which is seen in absorption is connected with the $K = 0$ excitons and is described by the C_{10} coefficient. The photoluminescence (PL) is connected with the indirect minimum of the Rashba exciton dispersion at K_R (see Fig.1). This leads to the additional negative diamagnetic shift described by the G_{10} coefficient. As a result the total diamagnetic shift of the exciton line in PL is described by the sum $C_{10} + G_{10}$. Calculations were conducted using material parameters in Table I and the exciton parameters in Table A1; panel **c** shows the calculation for Rashba splitting only in the conduction band, while panel **d** shows the results calculated with Rashba splitting in both the conduction and valence bands.

Table I and the calculated exciton parameters for different layer thickness in Table A1. Panels **a** and **b** of the figure depict 2D perovskites with 1 and 2 monolayer thickness, respectively. For layers thicker than 1 ML, we assume that the Rashba coefficients and effective masses are unchanged from the single ML values in Table I. Panel **c** shows the calculation of the diamagnetic shift for Rashba splitting only in the conduction band, while panel panel **d** shows the results calculated with Rashba splitting in both the conduction and valence bands. The coefficient C_{10} is identical in these two cases. This is the diamagnetic shift that would be observed in absorption since it is connected with the direct $K = 0$ excitons. However, the correction G_{10} connected to the Rashba terms differ for the two cases as it is associated with the indirect minimum in the exciton dispersion (see Fig.1) which occurs at different values for the different Rashba parameters. For the calculation in panel **c**, with Rashba coefficients $\alpha^e = 187$ meV·nm and $\alpha^h = 0$, the indirect minimum occurs at $K_R = 0.42\text{nm}^{-1}$ while in panel **c**, when $\alpha^e = 187$ meV·nm and $\alpha^h = -82$ meV·nm, the position, K_R, of the indirect minimum is nearly unchanged as a function of layer thickness, at $K_R \approx 0.61\text{nm}^{-1}$. Since photoluminescence is connected with the indirect minimum of the Rashba exciton dispersion at K_R , the total diamagnetic shift of the exciton line in PL is described by the sum $C_{10} + G_{10}$ shown in Fig. 6.

V. SUMMARY

The search for 2D and bulk semiconductors with large Rashba spin-orbit terms is stimulated by the usefulness of such materials in multiple opto-electronic applications including spintronic and quantum computing. In many device applications these terms allow replacement of operations that traditionally require an external magnetic field to be performed using an external electric field, which is much easier to apply and whose application does not require low temperature operation. The most obvious examples of such use of the Rashba terms is electron spin manipulation by electric fields, [9, 36] and in chiral structures, where spin-selective absorption and emission could be realized without external magnetic fields [37–41] Unfortunately, large Rashba terms are often connected with surface asymmetry and its origin and magnitude is very difficult to control. [42–44]

In this article we show two experimentally reliable rather simple magneto-optical measurements which could be used to confirm the existence of Rashba terms in the spectra of

electrons and holes even in samples of unoptimal quality, where the exciton line width is comparable to or larger than the Landau level splitting. The first of these is MCD, where a giant MCD signal should be observed at the energy gap band edge in the presence of Rashba terms. The second is the comparison of the exciton diamagnetic shift measured in absorption and photoluminescence. We hope that these simple approaches can provide experimentalists with unique tools to confirm the existence of the Rashba terms in the spectra of multiple novel spintronic semiconductors.

ACKNOWLEDGMENTS

This journal article was supported primarily through the Center for Hybrid Organic Inorganic Semiconductors for Energy (CHOISE), an Energy Frontier Research Center funded by the Office of Basic Energy Sciences, Office of Science within the US Department of Energy. Calculations of the exciton fine structure and dispersion, diamagnetic shifts, Landau level structure and optical properties were conducted by P.C.S. and were supported through CHOISE. A. L. E. formulated the theory of the diamagnetic corrections associated with Rashba terms, and acknowledges support from the U.S. Office of Naval Research. P.C.S would like to thank the Department of Applied Physics and Materials Science at the California Institute of Technology for hosting him as a Guest, and thanks Z. Valy Vardeny for many stimulating discussions.

APPENDIX A: EXCITON BINDING ENERGY AND OSCILLATOR STRENGTH

We start with a description of the quasi-2D exciton in a 2D layered perovskite structure. The exciton relative motion is analyzed first neglecting Rashba splitting, Eq. (1) and the mixing term Eq.41; these effects are added once the basic 2D exciton structure is determined. In layered perovskite structures, the inorganic semiconductor layer, thickness d, is surrounded by organic layers with a lower dielectric constant. Consequently the internal motion of the exciton is modified by dielectric confinement, resulting in a modified electron-hole interaction potential. [45, 46] We describe this modified potential using the image charge method introduced by Hanamura *et al.* [47] and used previously to calculate exciton binding energies in layered 2D HOIPs by Hong *et al.*. [48] In terms of the relative radial coordinate

of the electron and hole in the plane, $\rho_{e,h}$, and the z-coordinates z_e, z_h of the electron and hole, the interaction potential can be written in CGS units,

$$V_{eh}^{\rm 3D}(\rho, z_e, z_h) = -\frac{e^2}{\varepsilon_i} \sum_{n=-\infty}^{n=\infty} \frac{q_n}{\sqrt{\rho_{e,h}^2 + (z_e - z_{h,n})^2}} \ , \tag{A1}$$

where $q_n = q_{-n} = [(\kappa - 1)/(\kappa + 1)]^{|n|}$ and $z_{h,n} = (-1)^{|n|} z_h + nd$, where,

$$\kappa = \varepsilon_i / \varepsilon_o \tag{A2}$$

is the dielectric contrast ratio, the ratio of the dielectric constants of the inorganic layer (ε_i) and the surrounding organic layer (ε_o). We note that the interaction potential Eq. (A1) is three-dimensional. We make an adiabatic approximation which assumes that the motion perpendicular to the inorganic layer is much faster than the relative electron-hole motion in the layer. Within this assumption we can derive an adiabatic potential $V_d(\rho)$ describing the relative electron-hole motion by averaging Eq. (A1) over the wavefunctions of the lowest energy confined electrons, $\psi_c(z_e) = \sqrt{2/d}\cos(\pi z_e/d)$, and holes, $\psi_v(z_h) = \sqrt{2/d}\cos(\pi z_h/d)$, in the inorganic layer, respectively:

$$V_d^{Ad}(\rho) = \int_{-d/2}^{d/2} \int_{-d/2}^{d/2} dz_e dz_h \psi_c^*(z_e) \psi_v^*(z_h) V_{eh}^{\rm 3D}(\rho, z_e, z_h) \psi_c(z_e) \psi_v(z_h) \ . \tag{A3}$$

This results in an effective Hamiltonian for the electron/hole relative motion given by,

$$\hat{H}_{0,\rm REL} = -\frac{\hbar^2 \nabla_\rho^2}{2\mu} + V_d^{Ad}(\rho) \ . \tag{A4}$$

To find the energy and the wavefunction of the various 2D exciton states identified by principle quantum number $n \geq 1$ and azimuthal quantum number m with $|m| \leq n - 1$, we use the variational procedure with 2D hydrogenic ansatz functions [49]. For the 1S ground state, with $n = 1$, $m = 0$ we have the ansatz function,

$$\varphi_{1,0}(\rho, \phi; a) = \frac{4}{a} \frac{1}{\sqrt{2\pi}} e^{-2\rho/a} \ , \tag{A5}$$

while for the excited states with $n = 2$, $m = 0, \pm 1$, which we denote as the 2S and 2P states respectively, we have,

$$\varphi_{2,0}(\rho, \phi; a) = \frac{4e^{-\frac{2\rho}{3a}}(1 - \frac{4\rho}{3a})}{3\sqrt{3}a} \frac{1}{\sqrt{2\pi}} \ ; \qquad \varphi_{2,\pm 1}(\rho, \phi; a) = \frac{8\sqrt{\frac{2}{3}}\rho e^{-\frac{2\rho}{3a}}}{9a^2} \frac{1}{\sqrt{2\pi}} e^{\pm i\phi} \ , \tag{A6}$$

TABLE A1. Exciton radius and energy for 1S, 2P, and 2S excitons calculated for a series of model 2D perovskite structures with thickness, d, ranging from 1-5 monolayers (ML), using the material parameters in Table I. The energies $E_{n,m}$ are given relative to the band gap, E_g. The parameter A_r, which pertains to the effect of Rashba splitting in the exciton internal motion of the 1S exciton, is calculated from the variationally optimized values for a_{10} and a_{21} using Eq. B3 (see Appendix B).

d(ML)	a_{10} (nm)	E_{10} (meV)	a_{21} (nm)	E_{21} (meV)	a_{20} (nm)	E_{20} (meV)	A_r
1	3.05	-313.5	1.73	-73.3	1.95	-59.9	0.249
2	3.78	-231.7	1.92	-65.9	2.14	-53.1	0.284
3	4.33	-190.	2.08	-60.2	2.3	-48.6	0.301
4	4.79	-163.6	2.23	-55.6	2.44	-45.1	0.311
5	5.19	-144.9	2.36	-51.9	2.57	-42.2	0.318

where for each case the effective Bohr radius is taken as a variational range parameter. These trial functions are used to compute the energy using,

$$E_{n,m}(a) = \int_0^{2\pi} \int_0^{\infty} \rho \, d\rho \, d\phi \; \varphi^*_{n,m}(\rho, \phi; a) \, \hat{H}_{0,\mathrm{REL}} \, \varphi_{n,m}(\rho, \phi; a). \tag{A7}$$

The variationally calculated energy for the 1S, 2S, and 2P exciton levels are shown in Fig. A1 for an idealized 2D perovskite modeled after PEPI, plotted versus the inorganic layer thickness, d. We note that due to the non-central force nature of the e/h interaction potential, Eq. (A1), the exciton in the 2D perovskite system is non-hydrogenic, as manifested by the fact that the effective Bohr radii for the 2S and the 2P levels are distinct. Table A1 gives the numerical values determined for a series of model structures with thickness, d ranging from 1-5 ML using the material parameters in Table I.

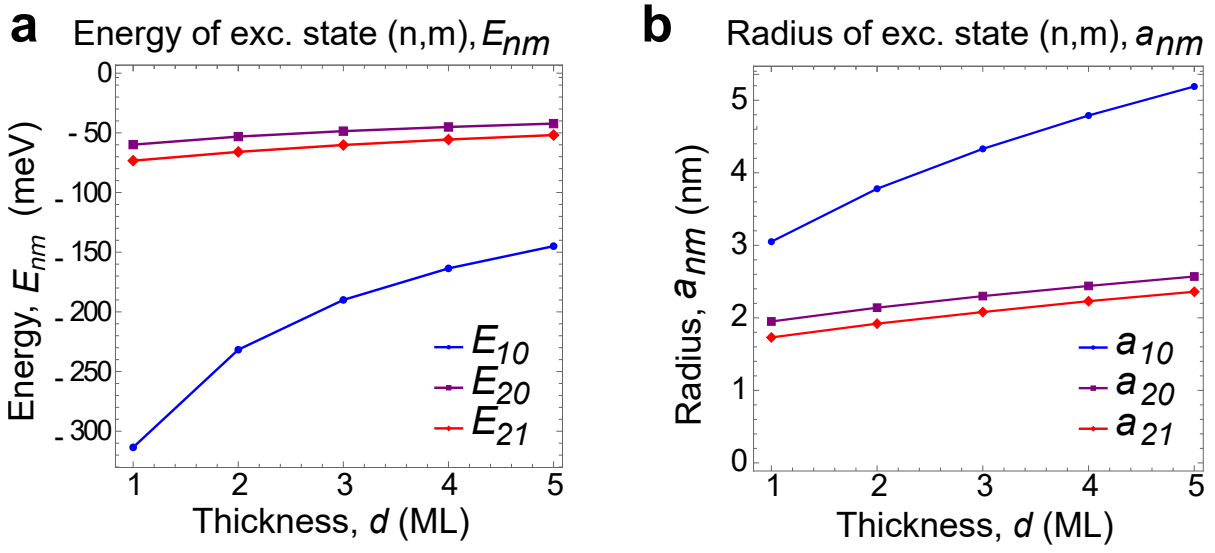

FIG. A1. Exciton binding energy and its radius versus inorganic layer thickness, d, in monolayers (MLs). Panel **a** shows the thickness dependence of the energy of the 1S, 2S and 2P excitons $E_{n,m}$ relative to the bandgap calculated for the exciton state with principal quantum number $n = 1, 2$ and angular momentum projection $m = 0, 1$. Panel **b** shows the thickness dependence of the effective radius of 2D exciton, $a_{n,m}$. Calculations are conducted for equal electron and hole effective mass equal to 0.174 m_0 with the interior dielectric $\epsilon = 5.4$ and dielectric contrast $\kappa = 2.11$ as summarized in Table I.

Using the variationally optimized wavefunctions, it is straightforward to find the matrix element $\langle 1S|\boldsymbol{r}|2P\rangle$ in Eq. (42) which is given by,

$$|\langle\varphi_{1,0}|x|\varphi_{2,1}\rangle| = |\langle\varphi_{1,0}|y|\varphi 2,1\rangle| = \frac{18\sqrt{6}a_{1,0}^3 a_{2,1}^2}{(a_{1,0}+3a_{2,1})^4} \ . \tag{A8}$$

The matrix element is the same for $|\langle\varphi_{1,0}|x|\varphi_{2,-1}\rangle|$.

With the exciton relative motion wavefunctions determined above we can also write expressions for the oscillator strength, $f^{\pm}_{n,m}$, per unit area, A, of the exciton states (n, m) for $\hat{\sigma}^{\pm}$ polarized light. For the 2P exciton the oscillator strength vanishes, since it is of odd parity. For the 1S and 2S excitons the oscillator strength per unit area is found from Eq. (25) and Bloch function definitions in Eqs. (22) - (23) as, [13]

$$\left(\frac{f^{\pm}_{1,0}}{A}\right) = \frac{E_p}{E_g + E_{10}}\cos^2\theta\ |\varphi_{1,0}(0)|^2\ ; \qquad \left(\frac{f^{\pm}_{2,0}}{A}\right) = \frac{E_p}{E_g + E_{20}}\cos^2\theta|\varphi_{2,0}(0)|^2\ . \tag{A9}$$

It is useful to note that since $|\varphi_{1,0}(0)|^2 = 8/\pi a_{10}^2$ and $|\varphi_{2,0}(0)|^2 = 8/27\pi a_{20}^2$, the oscillator strength of the excited 2S exciton level is substantially smaller than that of the lowest 1S level, even accounting for the different exciton radii of the two levels, which are given in Table A1. Neglecting the binding energy difference, the ratio of the oscillator strengths of the 2S to the 1S level is $\sim 9\%$ in a single layer perovskite.

APPENDIX B: EXCITON FINE STRUCTURE AND DISPERSION OF THE RASHBA EXCITON

The problem of the energy and center of mass dispersion of the Rashba exciton was solved in Swift *et al.*, Ref. [14]. Here we simply state the results. We define m_e, m_h as the electron and hole effective masses, with reduced effective mass μ defined in the usual way; and α_e, α_h as the electron and hole Rashba coefficients. We further adopt a quasi-tetragonal approximation for the 1S exciton fine structure [20, 22]. This results in the short-range exchange eigenvalues for the 1S exciton: $E_{0,0} = E_d = 0$, $E_{1,\pm1} = E_t = w\cos^2\theta$, and $E_{1,0} = E_z = 2w\sin^2\theta$ where $w = C\Theta$ with the short-range exchange constant C [29], and θ is defined in Eq. (24). Finally the overlap integral Θ is given by [50]

$$\Theta = \Omega \iint_V d^3r_e d^3r_h f^*(\boldsymbol{r}_e, \boldsymbol{r}_h)\delta(\boldsymbol{r}_e - \boldsymbol{r}_h) f(\boldsymbol{r}_e, \boldsymbol{r}_h) = \frac{3}{2d}\Omega|\varphi_{1,0}(0)|^2 \ , \tag{B1}$$

where Ω is the volume of unit cell and $\varphi_{n,m}(r)$ is the relative motion wavefunction of 2D exciton. Additionally, if Rashba splitting is present in both the conduction and valence bands, and if the inversion asymmetry is taken along the z direction, we find that the effect of Rashba splitting on the relative electron/hole motion takes the form of an effective electron-hole exchange interaction of the form, [14]

$$\hat{H}_R^{rel} = 2A_r\mathcal{E}_R\left(\hat{j}_x^e\hat{j}_x^h + \hat{j}_y^e\hat{j}_y^h\right) \ , \tag{B2}$$

where $\hat{j}_x^e$, $\hat{j}_y^e$ and $\hat{j}_x^h$, $\hat{j}_y^h$ are Pauli operators representing the electron and hole angular momentum projections along x, y; $\mathcal{E}_R = \alpha_e\alpha_h\mu/\hbar^2$ is the exciton Rashba energy; and A_r, which is a numerical coefficient whose value depends on the 1S and 2P exciton radii. This is given in Ref. [14] as,

$$A_r = 4a_{10}^2\frac{384a_{10}^2a_{2\pm1}^2}{(a_{10}+3a_{2\pm1})^6}\left(\frac{\frac{\hbar^2}{2\mu a_{10}^2}}{E_{1,0}(a_{1,0}) - E_{2,\pm1}(a_{2,\pm1})}\right) \ . \tag{B3}$$

Numerical values for A_r calculated from the variationally optimized values for a_{10} and a_{21} for a series of model 2D perovskite structures with thickness, d, ranging from 1-5 monolayers, using the material parameters in Table I, are tabulated in Table A1. The combined effect of SR exchange splitting and the internal motion Rashba terms above is then:

$$E_{0,0} = E_d = -4A_r\mathcal{E}_R, \quad E_{1,0} = E_z = 2w\sin^2\theta - 4A_r\mathcal{E}_R, \quad E_{1,1} = E_{1,-1} = E_t = w\cos^2\theta \tag{B4}$$

These expressions completely describe the fine structure of the lowest energy 1S exciton at zero center of mass motion. We note that if the electron and hole Rashba coefficients, α_e and α_h, respectively, have opposite signs, then the conduction electron and valence band electron coefficients have the same sign due to the sign inversion in going from the electron to the hole picture for the valence band. This, coupled with the fact that the angular momentum and the spin are anti-parallel for the conduction bands in perovskites implies that the spin textures are co-helical[15], i.e., the outer spin-split branches of the conduction and valence bands have parallel spins. In this case, $\mathcal{E}_R < 0$ which, depending on parameter values, can result in a level order inversion between the Z and D exciton at $K = 0$. To continue, we must determine the dispersion in the plane associated with center of mass K where $\boldsymbol{P} = \hbar\boldsymbol{K}$. A complete description of the exciton dispersion requires that we also include not only the exciton fine structure splitting due to electron-hole exchange and the internal motion Rashba terms as described in Eq. (B4), but additional terms connected to center of mass motion which mix the fine structure levels, resulting in the following Hamiltonian:

$$\hat{H}^{\text{Tetr}}_{\text{tot,}}(\boldsymbol{K}) = \hat{H}^{\text{Tetr}}_{\text{INT}} + \hat{H}^{\text{Tetr}}_{\text{COM}}(\boldsymbol{K}) \ , \tag{B5}$$

The Rashba term contribution to the COM motion, $\hat{H}_{R,\text{COM}}$ is:[51]

$$\hat{H}_{R,\text{COM}}(\boldsymbol{P}) = \frac{1}{M}\left[\left(m_e\frac{\alpha_e}{\hbar}\hat{j}^e_x + m_h\frac{\alpha_h}{\hbar}\hat{j}^h_x\right)P_y - \left(m_e\frac{\alpha_e}{\hbar}\hat{j}^e_y + m_h\frac{\alpha_h}{\hbar}\hat{j}^h_y\right)P_x\right] \ , \tag{B6}$$

The total exciton dispersion is described by diagonalizing Eq. (B5), giving the Rashba exciton dispersion. This is found to separate into two branches: Branch A, representing the coupled Z and $T(X,Y)$ excitons: [14]:

$$E^{\pm}_A(K) = \mathcal{E}_{0,0} + \frac{\hbar^2K^2}{2M} + \frac{E_t + E_z}{2} \pm \frac{\sqrt{(E_t - E_z)^2 + 4K^2(\alpha^+_{\text{ex}})^2}}{2} \ , \tag{B7}$$

while branch B represents the coupled D and T excitons: [14]:

$$E^{\pm}_B(K) = \mathcal{E}_{0,0} + \frac{\hbar^2K^2}{2M} + \frac{E_d + E_t}{2} \pm \frac{\sqrt{(E_d - E_t)^2 + 4K^2(\alpha^-_{\text{ex}})^2}}{2} \ . \tag{B8}$$

In these expressions, $\alpha_{\rm ex}^{\pm} = (\alpha_e m_e \pm \alpha_h m_h)/M$, where $M = m_e + m_h$ is the exciton total mass.

The exciton multiplet has its minimum energy $\mathcal{E}_{\rm min}$ on a circle in K-space defined by $K_x^2 + K_y^2 = K_R^2$, where for the case that α_e and α_h have opposite signs, or if $\alpha_e \neq 0$ and $\alpha_h = 0$, the minimum occurs on branch B^-, and has its minimum at K_R with energy given by,

$$\mathcal{E}_{\rm min}^B = \mathcal{E}_{0,0} + \frac{E_d + E_t}{2} - \frac{M(\alpha_{\rm ex}^-)^2}{2\hbar^2} - \frac{(E_d - E_t)^2\hbar^2}{8M(\alpha_{\rm ex}^-)^2} \ , \quad K_R^2 = \frac{(M\alpha_{\rm ex}^-)^2}{\hbar^4} - \frac{(E_d - E_t)^2}{4(\alpha_{\rm ex}^-)^2} \ . \quad \text{(B9)}$$

The dispersion of the Rashba exciton shown in Fig. 1 **b** and **c** have indirect minima. The dispersion is calculated for two set of parameters describing a single mono-layer HOIP. Panel **b** shows the exciton dispersion calculated for non-zero Rashba coefficient in the conduction band, $\alpha_e \neq 0$. In panel **c** the calculations are conducted for the both Rashba coefficients not equal to zero. In the last case α_e and α_h have opposite signs, corresponding to co-helical spin textures in the conduction and valence bands, as expected from DFT calculations in 2D perovskites [16] and three-dimensional perovskites [52]. This results in a level order inversion between the Z and D exciton as described above in Eq. (B4).

---

[1] R. P. Seisyan and B. P. Zakharchenya, Interband magneto-optics of semiconductors as diamagnetic exciton spectroscopy, Ch. 7 in "Landau Level Spectroscopy", Ed. G. Landwehr and E. I. Rashba, Elsvier Science Publishers B. V., 1991.

[2] L. A. Falkovsky, Quantum magneto-optics of the graphite family, *Journal of Experimental and Theoretical Physics*, **115** 1151-1164 (2012).

[3] G. Wang, L. Bouet, M. M. Glazov, T. Amand, E. L. Ivchenko, E. Palleau, X. Marie and B. Urbasze, Magneto-optics in transition metal diselenide monolayers. *2D material*, **2**, 0344002, 2015.

[4] Al. L. Efros, L. M. Kanskaya, S. I. Kokhanovskii, and R. P. Seisyan, Indium antimonide energy band parameters derived from diamagnetic exciton spectra, *Solid State Commun.*, **43**, 613 -617 (1982).

[5] D. M. Hofmann, K. Oettinger, Al. L. Efros, and B. K. Meyer, Magnetic circular dichroism study of heavy and light hole g-factors in InGaAs/InP quantum wells, *Phys. Rev. B*, **55**, 9924 -9928 (1997).

[6] Y. A. Bychkov and E. I. Rashba, Properties of a 2D electron gas with lifted spectral degeneracy, *JETP Lett.*, **39**, 78 (1984).

[7] E. I. Rashba, Properties of semiconductors with an extremum loop. I. Cyclotron and combinational resonance in a magnetic field perpendicular to the plane of the loop, *Sov. Phys. Solid State* ,**2**, 1109-1122 (1960).

[8] M. A, Becker, R. Vaxenburg, G. Nedelcu, P. C. Sercel, A. Shabaev, M. J. Mehl, J. G. Michopoulos, S. G. Lambrakos, N. Bernstein, J. L. Lyons, T. Stöferle, R. F. Mahrt, M. V. Kovalenko, D. J. Norris, G. Rainò, Al. L. Efros, Bright triplet excitons in caesium lead halide perovskites, *Nature*, **553**, 189-193 (2018)

[9] E. I. Rashba and Al. L. Efros, Orbital mechanisms of electron spin manipulation by an electric field, *Phys. Rev. Lett.*, **91**, 126405 (2003).

[10] M. Dyksik, H. Duim, D. K. Maude, M. Baranowski, M. A. Loi, P. Plochocka, Brightening of dark excitons in 2D perovskites, *Sci. Adv.*, **7**, eabk0904 (2021).

[11] Z. G. Yu, Effective-mass model and magneto-optical properties in hybrid perovskites, *Sci. Rep.*, **6**, 28576 (2016).

[12] U. N. Huynh, Y. Liu, A. Chanana, D.R. Khanal, P.C. Sercel, J.Huang, and Z.V.Vardeny, Transient quantum beatings of trions in hybrid organic tri-iodine perovskite single crystal, *Nat. Commun.*, 13, 1428 (2022).

[13] P. C. Sercel, "Theory of excitons in metal halide perovskites", in Hybrid Organic Inorganic Perovskites: Physical Properties and Applications (In 4 Volumes), Vol.1 (World Scientific 2022).

[14] M W. Swift, J. L. Lyons, Al. L. Efros, and P. C. Sercel, Rashba exciton in a 2D perovskite quantum dot, *Nanoscale*, **13**, 16769 -16769 (2021).

[15] F. Zheng, L.Z. Tan, S. Liu, and A. M. Rappe, Rashba spin-orbit coupling enhanced carrier lifetime in $CH_3NH_3PbI_3$, *Nano Lett.*, **15**, 7794-7800 (2015).

[16] J. Yin, P. Maity, L. Xu, A.M. El-Zohry, H. Li, O. M. Bakr, J.-L. Bredas, and O. F. Mohammed, Layer-dependent Rashba band splitting in 2D hybrid perovskites, *Chem. Mater.*, **30**, 8538-8545 (2018).

[17] J.-C. Blancon, A. V. Stier, H. Tsai, W. Nie, C. C. Stoumpos, B. Traoré, L. Pedesseau, M. Kepenekian, F. Katsutani, G. T. Noe, J. Kono, S. Tretiak, S. A. Crooker, C. Katan, M. G. Kanatzidis, J. J. Crochet, J. Even and A. D. Mohite, Scaling law for excitons in 2D perovskite

quantum wells, *Nature Commun.* **9**, 2254 (2018).

[18] M. Dyksik, S. Wang, W. Paritmongkol, D. K. Maude, W. A. Tisdale, M. Baranowski, and P. Plochocka, Tuning the excitonic properties of the 2D $(PEA)_2(MA)_{n-1}Pb_nI_{3n+1}$ perovskite family via quantum confinement, *J. Phys. Chem. Lett.* **12**, 1638-1643 (2021).

[19] A. Fieramosca, L. De Marco, M. Passoni, L. Polimeno, A. Rizzo, B. L. T. Rosa, G. Cruciani, L. Dominici, M. De Giorgi, G. Gigli, L. C. Andreani, D. Gerace, D. Ballarini, and D. Sanvitto, Tunable out-of-plane excitons in 2D single-crystal perovskites, *ACS Photonics* **5**, 4179-4185 (2018).

[20] M. Steger, S.M. Janke, P.C. Sercel, B.W. Larson, H. Lu, X. Xin, V. Yu, V. Blum, and J.L. Blackburn, On the optical anisotropy in 2D metal-halide perovskites, *Nanoscale*, **14**, 752-765(2022).

[21] Y. Zhai, S. Baniya, C. Zhang, J. Li, P. Haney, C.-X. Sheng, E. Ehrenfreund, Z. V. Vardeny, Giant Rashba splitting in 2D organic-inorganic halide perovskites measured by transient spectroscopies *Sci. Adv.*, 3: e1700704 (2017).

[22] K. Tanaka, T. Takahashi, T. Kondo, K. Umeda, K. Ema, T. Umebayashi, K. Asai, K. Uchida and N.Miura, Electronic and excitonic structures of inorganic–organic perovskite-type quantum-well crystal $(C_4H_9NH_3)_2PbBr_4$ *Jpn. J. Appl. Phys., Part 2*, **44**, 5923-5932 (2005).

[23] C. Harkort, D. Kudlacik, N. E. Kopteva, D. R. Yakovlev, M. Karzel, E. Kirstein, O. Hordichuk, M. Kovalenko, and M. Bayer, Spin-flip raman scattering on electrons and holes in two-dimensional $(PEA)_2PbI_4$ perovskites, *Small*, 2300988 (2023).

[24] D. B. Straus, S. H. Parra, N. Iotov, Q. Zhao, M. R. Gau, P. J. Carroll, J. M. Kikkawa, and C. R. Kagan, Tailoring hot exciton dynamics in 2D hybrid perovskites through cation modification, *ACS Nano*, **14**, 3621-3629 (2020).

[25] S. Neutzner, Felix Thouin, D. Cortecchia, A. Petrozza, C. Silva, and A. R. S. Kandada, Exciton-polaron spectral structures in two-dimensional hybrid lead-halide perovskites, *Phys. Rev. Materials*, bf 2, 064605 (2018).

[26] K. Posmyk, N. Zawadzka, M. Dyksik, A. Surrente, D. K. Maude, T. Kazimierczuk, A. Babinski, M. R. Molas, W. Paritmongkol, M. Maczka, W. A. Tisdale, P. Płochocka, and M. Baranowski, Quantification of exciton fine structure splitting in a two- dimensional perovskite compound, *J. Phys. Chem. Lett.*, **13**, 4463-4469 (2022).

[27] D. Tong, The Quantum Hall Effect, TIFR Infosys Lectures, arXiv:1606.06687v2

[28] J. O. Dimmock, Introduction to the theory of exciton states in semiconductors, in *Semiconductors and Semimetals, vol. 3*, edited by R. K. Willardson and A. C. Beer, Academic Press, New York, (1967).

[29] P. C. Sercel, J. L. Lyons, D. Wickramaratne, R. Vaxenburg, N. Bernstein, N.; A. L. Efros, Exciton fine structure in perovskite nanocrystals, *Nano Lett.*, **19**, 4068- 4077 (2019).

[30] E.O. Kane, Band structure of Indium Antimonide, *J. Phys. Chem. Solids*, **1**, 249-261 (1957).

[31] A. Miyata, A. Mitioglu1, P. Plochocka, O. Portugall, J. T.-W. Wang, S. D. Stranks, H. J. Snaith, and R. J. Nicholas, Direct measurement of the exciton binding energy and effective masses for charge carriers in organic–inorganic tri-halide perovskites, *Nat. Phys.* **11**, 582-588 (2015).

[32] L. C. Andreani, Optical transitions, excitons, and polaritons in bulk and low-dimensional semiconductor structures, in Confined Electrons and Photons Edited by E. Burstein and C. Weisbuch, Plenun Press, New York, 1995.

[33] M. Shinada and S. Sugano, Interband optical transitions in extremely anisotropic semiconductors. I. Bound and unbound exciton absorption, *J. Phys. Soc. Jpn.*, **21**, 1936 (1966).

[34] T. Szkopek, Optical frequency conductance, susceptance and admittance of quantum wells. *IEEE J Quantum Electron* **47** 500–509 (2011).

[35] L. P. Gor'kov, and I. E. Dzyaloshinskii. Contribution to the theory of the Mott exciton in a strong magnetic field. *Soviet Phys. JETP*, **26**, 449-451 (1968).

[36] Y. Kato, R. C. Myers, D. C. Driscoll, A. C. Gossard, J. Levy, and D. D. Awschalom, Gigahertz electron spin manipulation using voltage-controlled g-tensor modulation, *Science*,**299**, 1201-1204, (2003).

[37] G. Long, C. Jiang, R. Sabatini, Z. Yang, M. Wei1, L. N. Quan, Q. Liang, A. Rasmita, M. Askerka, G. Walters, X. Gong, J. Xing, X. Wen, R. Quintero-Bermudez, H. Yuan, G. Xing, X. R. Wang, D. Song, O. Voznyy, M. Zhang, S. Hoogland, W. Gao, Q. Xiong and E. H. Sargent, Spin control in reduced-dimensional chiral perovskites, *Nat. Photonics*, **12** 528-533 (2018).

[38] G. Long, R. Sabatini, M. I. Saidaminov, G. Lakhwani, A. Rasmita, X. Liu, E. H. Sargent, and W. Gao, Chiral-perovskite optoelectronics, *Nat. Rev. Mater.*, **5**, 423-439 (2020).

[39] M. K. Jana, R. Song, H. Liu, D.R. Khanal, S.M. Janke, R. Zhao, C. Liu, Z. V. Vardeny, V. Blum, and D.B. Mitzi, Organic-to-inorganic structural chirality transfer in a 2D hybrid perovskite and impact on Rashba-Dresselhaus spin-orbit coupling, *Nat. Commun.*, 11, 4699 (

2020).

[40] M. K. Jana, R. Song, Y. Xie, R. Zhao, P.C. Sercel, V. Blum, and D.B. Mitzi, Structural descriptor for enhanced spin-splitting in 2D hybrid perovskites *Nat. Commun.*, 12, 4982 (2021).

[41] J. Crassous, M. J. Fuchter, D. E. Freedman, N. A. Kotov, J. Moon, M. C. Beard, and S. Feldmann, Materials for chiral light control, *Nat. Rev. Mater.*,https://doi.org/10.1038/s41578-023-00543-3 (2023).

[42] D. Niesner, M. Wilhelm, I. Levchuk, A. Osvet, S. Shrestha, M. Batentschuk, C. Brabec, and T. Fauster, Giant Rashba splitting in $CH_3NH_3PbBr_3$ organic-inorganic perovskite, *Phys. Rev. Lett.*, **117**, 126401 (2016).

[43] M. Isarov, L. Z. Tan, M. I. Bodnarchuk, M. V. Kovalenko, A. M. Rappe, and E. Lifshitz, Rashba effect in a single colloidal $CsPbBr_3$ perovskite nanocrystal detected by magneto-optical measurements, *Nano Lett.*, **17**, 5020-5026 (2017).

[44] D. Weinberg, Y. Park, D. T. Limmer, and E. Rabani, Size-dependent lattice symmetry breaking determines the exciton fine structure of perovskite nanocrystals, arXiv:2303.00707 (2013), https://doi.org/10.48550/arXiv.2303.00707.

[45] N. C. Ritova, Screened potential of a point charge in a thin film, *Vestnik of Moskow University*, **N3**, 30 (1967). Translated to English in, https://arxiv.org/abs/1806.00976.

[46] L. V. Keldish, Coulomb interaction in thin semiconductor and semimetal films,*JETP Lett.*,**29**, 658-661 (1979).

[47] E. Hanamura and N. Nagaosa, Quantum well with enhanced exciton effects and optical nonlinearity, *Mater. Sci. Eng. B*, 1988, **1**, 255-258

[48] X. Hong, T. Ishihara and A. U. Nurmikko, Dielectric confinement effect on excitons in PbI_4-based layered semiconductors, *Phys. Rev. B.*, **45**, 6961–6964 (1992).

[49] X. L. Yang, S. H. Guo, F. T. Chen, K. W. Wong, and W. Y. Chin, Analytical solution of a two-dimensional hydrogen atom. I. Nonrelativistic case, *Phys. Rev. A* **43** 1186-1196 (1991).

[50] M. Gramlich, M. W. Swift, J. L. Lyons, A. L. Efros, P. C. Sercel, A. Urban, Dark and bright excitons in halide perovskite nanoplatelets, *Adv. Sci.*, DOI: 10.1002/ADVS.202103013 (2021).

[51] P. C. Sercel, Z. V. Vardeny, and A. L. Efros, Circular dichroism in non-chiral metal halide perovskites, *Nanoscale* **12**, 18067-18078 (2020).

[52] X. Zhang, J.-X. Shen, and C. G. Van de Walle, Three-dimensional spin texture in hybrid perovskites and its impact on optical transitions *J. Phys. Chem. Lett.*, **9**, 2903-2908 (2018).